A STUDY OF ALIGNABILITY OF MEMS BASED OPTICAL CROSSBAR SWITCHES

by

Dilip Gulati

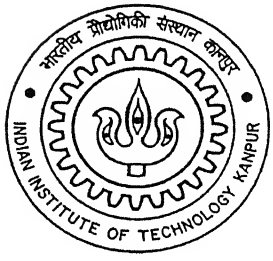

Center for Laser Technology

INDIAN INSTITUTE OF TECHNOLOGY, KANPUR

June 2005

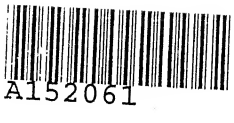

A STUDY OF ALIGNABILITY OF MEMS BASED OPTICAL CROSSBAR SWITCHES

A Thesis Submitted

in Partial Fulfillment of the Requirements

for the Degree of

Master of Technology

by

Dilip Gulati

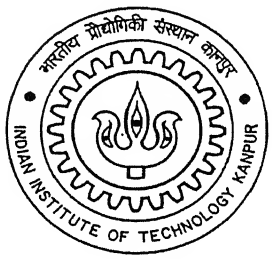

to the

Center for Laser Technology

INDIAN INSTITUTE OF TECHNOLOGY,KANPUR

June 2005

CERTIFICATE

It is certified that the work contained in the thesis entitled "*A study of alignability of MEMS based optical crossbar switches*" by *Dilip Gulati* has been carried out under my supervision and that this work has not been submitted elsewhere for a degree.

(Anjan K.Ghosh)

June 2005

Head of Department,

Department of Electrical Engineering,

Indian Institute of Technology,

Kanpur-208016.

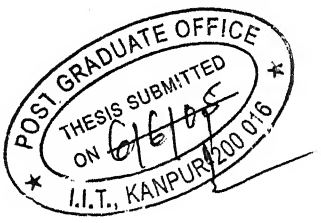

Abstract

The use of free space optical interconnects for short distance communication between integrated circuits or boards in distributed digital system has attracted considerable interest in recent years. Free space optical interconnects offer a scalable approach in achieving high-data-rate, large bandwidth, low power connections. However, free space optical interconnect requires careful assembly in order to maintain end-to-end alignment. The successful development, fabrication and deployment of optical interconnect depend on how easily the components of the interconnect can be aligned and how tolerant the interconnects is to misalignments. An interconnection system which is difficult or time consuming to align is costly to develop and fabricate and may be unstable. The statistical measure of the ease with which an optical interconnect can be aligned has been developed is called alignability, uses the efficiency of power transfer as a measure of alignment quality.

In this thesis the alignability definition is implemented for a simple MEMS based optical crossbar switch. Sensitivity of alignability with respect to different parameters of switch has also been estimated . This analysis could be useful in characterizing the alignment of MEMS based optical crossbar switches and obtaining design guidelines.

To My Parents

Acknowledgements

I would like to thank my advisor Dr. Anjan K. Ghosh, for his guidance and support throughout the course of my graduate program. Dr. Ghosh has always given me a patient hearing and his immense experience and wisdom has taught me how to ask questions and express my ideas more effectively. He showed me different ways to approach a research problem and the need to be persistent to accomplish any goal.

I would like to express my gratitude to my friends Hurry, Jawahar, Mayank, Pulkit and Vijay for inspiring me throughout the course of the thesis. I would like to specially thank to Raghu and Rajesh for sharing their knowledge for the completion of my thesis.

I like to say thanks to my classmates Ajay, Bedi, Neha, Sumathi and Vinay for their wonderful company throughout the course.

Lastly, I would like to thank my family for their love and support and share this moment of happiness with my mother, father and brothers.

Contents

List of Figures

Chapter 1

Introduction

With the continuing drive towards higher speed, density and functionality in electronics, electrical interconnects became inadequate. The possibility of using optical interconnects to meet the increasingly higher speed and density requirements which surpass the ability of electrical interconnects is due to optics' high speed, bandwidth, freedom from capacitative loading effect, crosstalk and electromagnetic interference. Fabrication and assembly of an optical interconnect requires precise alignment of the light beam and devices. Free Space Optical Interconnects (FSOIs) can provide parallel and high bandwidth optical interconnects with simple and compact optical systems. Various configurations of optical interconnects have been studied. In order to choose the proper optical configurations, the analysis of alignment tolerance has to be investigated. An optical interconnect that is difficult to align will be costly to manufacture and deploy. A measure of the ease with which an optical interconnect can be aligned is called Alignability[1], uses the efficiency of power transfer in the interconnect to

determine the quality of the alignment. A higher value of alignability indicate the ease of aligning an optical interconnect.

1.1 Comparison between electrical interconnects and optical interconnects

Conventionally, communication or data exchange between computers, telecommunication and data-communication systems take place through metallic wires or tracks known as electrical interconnects. But due to the considerable increase in performance requirements of the above systems, large-scale electronic systems now suffer from an interconnection bottleneck. Electrical interconnects are limited by capacitative loading, crosstalk between closely spaced interconnects, planer or quasi-planer constraints for PCBs and ICs, and, in situation which call for parallel communication. Optical interconnects can provide higher speed and density than electrical interconnects because optics give us high bandwidth, freedom from capacitative loading effects and crosstalk.

Despite many benefits of these optical interconnects, diffraction has always been a problem. Diffraction effects exist when a light beam passes through a finite aperture. Another problem that lies under the design of FSOI system is the packaging of FSOI's. Alignment of optoelectronic and optical components during assembly is a key factor when determining the feasibility and the performance of the whole system. In addition to substituting a light channel (could be free space or a waveguide)for an electrical channel, replacing a single wire or circuit trace with an optical interconnect requires

at the very minimum, two additional components : an optical source and an optical detector. Usually, more components such us lenses, holographic elements, mirrors, optical fibers, *etc* are also required.

Fabrication and assembly of an optical interconnect, with all of these components, requires precise alignment of light beams and devices. Because of the 3-D, non-contact nature of free space optics, and the increasing number of components, achieving the alignment necessary for the interconnect to operate correctly and reliably a is more difficult task than that of simply connecting a wire between two points. Alignment of an optical interconnect involves angular, longitudinal, and transverse positioning of the optical and electrooptic components. The successful development, fabrication and deployment of optical interconnects depend on how easily the components of the interconnect can be aligned and/or how tolerant the interconnect is to misalignments. An interconnection system which is difficult or time consuming to align is costly to develop and fabricate and may be unstable.

Any optical or optoelectronics system consists of interconnects so the alignment issue is of prime importance for any kind of optical system in order to realize a reliable and low loss system.

1.2 Free space optical interconnects design

The introduction of free space optical interconnects eliminates the need for the propagating medium completely. A simple form of FSOI would require an emitting source

on one end and a detector or receiver on the other end. This setup is also called Basic Optical Interconnect(BOI) which is illustrated in Figure 1.1. Alignability calculation has been done for BOI [1].

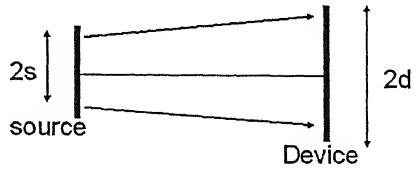

Figure 1.1: Basic Optical Interconnect

Figure 1.2 shows a practical optical interconnect model in which the light beam from the input fiber is collimated by a lens and is incident on an inclined mirror, which directly reflects the beam to an other collimating lens, after transmitting through this lens the beam is now collected by the detector.

1.3 Optical Cross Connect

A graphical drawing of 8x8 OXC is seen in Figure 1.3. Its a typical example of an optical MEM system. The eight input fibers to be switched come from the left side. This system implements a true cross-bar switch, where each input can be routed to any of the output fibers, lined across the bottom of the chip. In order to make every connection available, there are 64 hinged mirrors lying on the surface of the chip. As an interconnection is desired, the specified mirror that can complete the interconnect is lifted off the surface, using conventional MEM components such as scratch drive

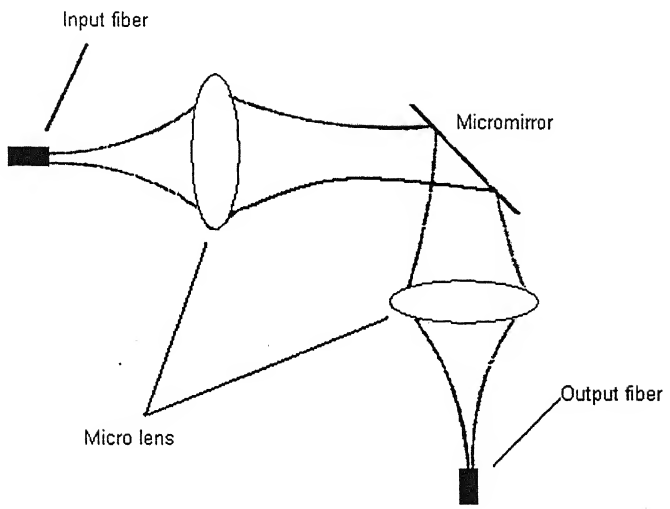

Figure 1.2: Optical Interconnect

actuators (SDA), into a standing position with a 45 degree angle relative to the incoming light. In the figure, two example interconnects are completed, the black mirrors represent mirrors that are standing and the grey mirrors represent mirrors that remain lying down. The sizes of the components and the propagation distances between the components constrain the optical propagation model.

Alignability definition could be extended for an array of optical but in this thesis we have studied alignability for an single optical interconnect as illustrated in Figure 1.2.

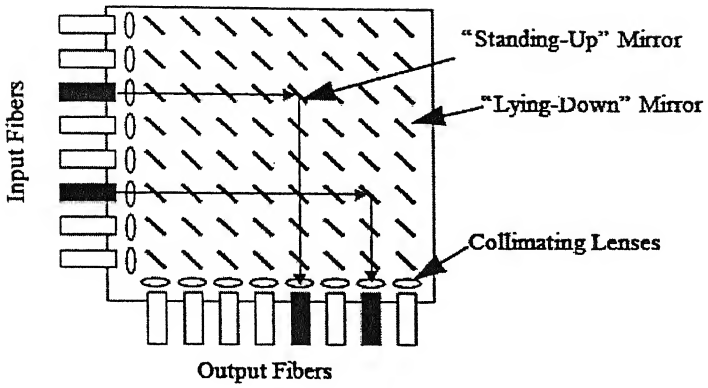

Figure 1.3: Free-Space MEM Optical Switch

1.4 Thesis Outline

Chapter 2 introduces the development of the definition of Alignability. In the *chapter 3* background theory for calculating the alignability of MEMS based optical crossbar switch has been discussed. *Chapter 4* analyzes the switch for evaluating the amplitude distribution at different positions of the switch. Alignability for a MEMS based optical crossbar switch has been estimated in *Chapter 5* and in *Chapter 6* alignability results has been analyzed.

Chapter 2

Background of Alignability

Alignability[1] is a probability based measure of the ease with which the components of an optical interconnect can be aligned. The alignability measure is intended to aid in optical interconnect package design by allowing a quantitative comparison of different designs. The alignability depends upon various interconnect design and packaging parameters, including component size, the beam's spot size, and the standard deviations of alignment offsets.

Development of the definition of alignability is based upon a rudimentary optical interconnect which we call a basic optical interconnect (BOI). The BOI consists of a single light beam, with a circular cross-section, and a single flat device, also with a circular cross-section, such as photodiode or a clear aperture. More complex and practical interconnects can be modeled as the series and parallel combination of a number of BOIs.

The alignment of the BOI requires that the beam (light source) and device be

positioned so that the power transfer from the beam to the device is maximized. The efficiency of the BOI, defined as the ratio of the power received by device to the total power in beam, is used to determine how well the BOI has been aligned. Various random offsets in the positioning of the beam and device results in misalignment and a change in the BOI efficiency.

Considering only one alignment offset at a time, the dependence of the efficiency on the offset allows us to obtain the probability of aligning the BOI such that its efficiency is greater than or equal to a given value. This probability will be denoted by $P_\xi(\eta)$, where ξ is the alignment offset being considered and η is the given lower limit on the efficiency. If the BOI design or fabrication is altered so that the offsets are reduced or the efficiency is less sensitive to the offsets, than $P_\xi(\eta)$ should increase. Also, a BOI should be easier to align if its efficiency is less sensitive to offsets or the offsets tend to be inherently smaller. Thus, a probability based measure of the ease of alignment, the alignability, can be defined as a function of $P_\xi(\eta)$.

2.1 Probability distribution of alignment

The process of BOI alignment results in three different types of random offsets:longitudinal, lateral, and angular as shown in Figure 2.1. Because both the source and the device may have offsets, a BOI will have two of each type of offset for a total of six possible offsets. The standard deviations of the alignment offsets depend on several BOI cost factors: the time spend on the alignment, the design and quality of the holders, posi-

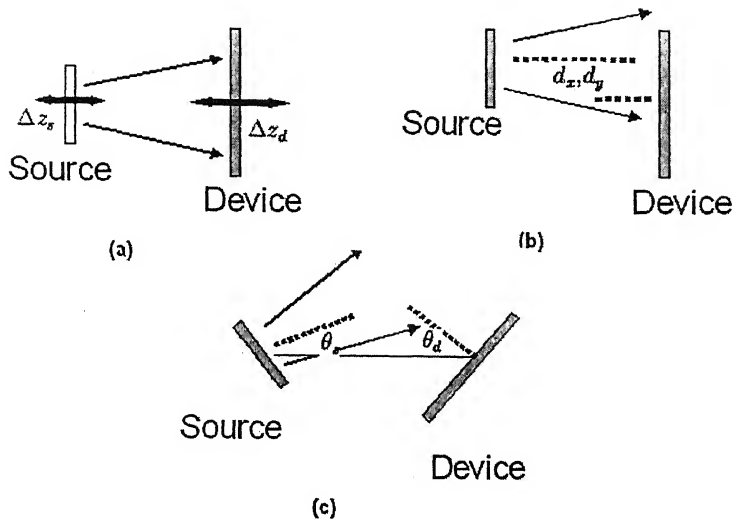

Figure 2.1: Schematic illustration of the three types of offsets in an optical interconnect: (a)longitudinal, (b)transverse, and(c)angular. Each type of offset may occur at the source and device

tioners, and other auxiliary devices used to position and hold the device, the sizes of the device and the beam, and the degree of freedom of the positioners. All of these factors can be grouped together into an overall cost measure (OCM). As the OCM increases, by increasing the time spent on the alignment, for instance, we expect the standard deviations of the offset to decrease. Thus, the OCM and the standard of an offset are inversely proportional to another as Equation 2.1

$$\sigma = \frac{K}{OCM} \tag{2.1}$$

where K is the proportionality constant for the given offset.

Presently, we use a heuristic model to define the OCM.

$$Overallcostmeasure = \alpha_1 t c_o + \alpha_2 D c_p + \alpha_3 d + \alpha_4 s + \alpha_5 g(\lambda) \tag{2.2}$$

where t= the lime spent on alignment, c_o=the hourly wage (cost) of the operator (proportional to skill), D = the degrees of freedom in the holders, positioners, and other auxiliary devices, d and s are the radii of the device and the beam respectively, and g(λ) is a nonlinear function of the source wavelength. Parameters $\alpha_1, \alpha_2, ...\alpha_5$ are regression constants.

To determine the alignability, we need to estimate the probability density functions (pdfs)of the alignment offset. Considering that we are dealing with a large number of random variables and the offsets are caused by several independent random factors, the central limit theorem leads us to assume that the pdfs are Gaussian. Thus we can approximate the pdf of any of the alignment offset (arbitrarily labeled x) as

$$f_x(x) = \frac{1}{\sigma_x \sqrt{2\Pi}} exp\left[\frac{-x^2}{2\sigma_x^2}\right] \tag{2.3}$$

where σ_x denotes the standard deviation of one of the six offsets. As noted in Equation 2.3, the standard deviation is related to the OCM of the BOI. Thus, the pdfs of the offsets are functions of the OCM of the BOI.

2.2 Probability of BOI efficiency

The efficiency of the BOI depends not only on alignment offsets, but also on beam and device parameters. This functional dependence is shown in the following

$$\eta(s, d, \lambda, \theta, \beta, \Delta z, x, y, z) = \frac{received\ power}{total\ beam\ power} \tag{2.4}$$

where s and d are the beam spot size and device size respectively, λ = the wavelength of the beam, β = the beam divergence, θ = angular offset, x and y are the transverse offsets, Δz longitudinal offset, and z = source-to-device separation. The form of the right hand side of equation 2.4 will depend on the intensity and responsively profiles of the beam and device respectively and the shapes of the beam and device.

To simplify the analysis, We will be considering only one offset at a time, we will denote this single, arbitrary offset by ξ. Figure 2.2 illustrate how efficiency varies as a function of this offset (in this case chosen to be transverse offset). In Figure 2.2, by the three different curves, we show how the $\eta(\xi)$ versus ξ curve can change if one of the other BOI parameters (device size in Figure 2.2) is changed. For all cases, higher efficiency requires smaller offsets. And, in some cases (see Figure 2.2a with d=$s/2$) the efficiency has a peak value which is less than one; even for zero offset(note : although only positive offsets are shown in Figure 2.2, negative offsets are also valid though they are not shown because the curves are symmetric about the efficiency axis). By restricting the efficiency dependence to one offset at a time, we are able to invert Equation 2.4 to find the maximum allowed offset for a given BOI efficiency. $\eta(\xi)$ versus

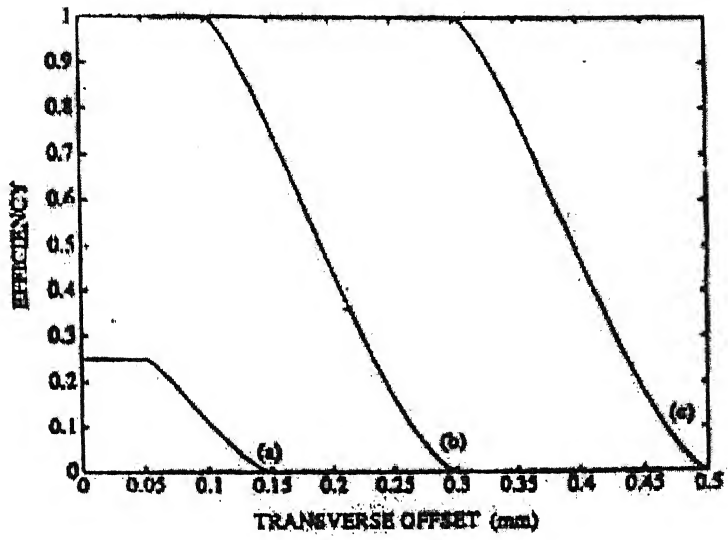

Figure 2.2: BOI efficiency versus transverse offset: (a) $d = 0.05$mm, (b) $d = 0.2$mm, (c) $d = 0.4$mm. The spot size $s = 0.1$ mm for all three curves [1]

ξ. By exchanging the axes of Fig 2.2, *ie* taking efficiency to be the independent variable and taking transverse offset to be the dependent variable, we can get an idea of the form of this function. For convenience, the data of Figure 2.2 has been plotted in Fig 2.3, with the axes exchanged.

For the general BOI which we are considering the function $\eta(\xi)$ versus ξ will produce two values one negative (ξ^-) and one positive(ξ^+), for most offsets. Because these values represents the maximum offset for which the efficiency $= \eta$, any value of the offset, ξ, that is between ξ^- and ξ^+ will yield an efficiency which is grater than, or equal to, η. Thus by integrating the pdf of the offset Equation 2.3, from ξ^- to ξ^+, we obtain the probability of the BOI having an efficiency which is greater than, or equal

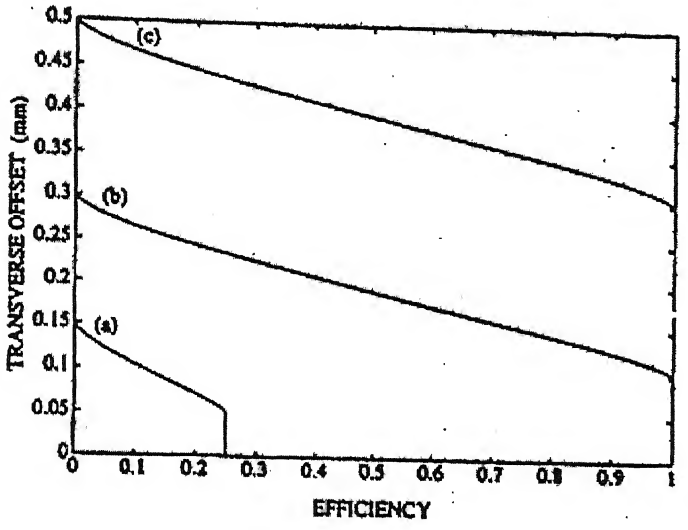

Figure 2.3: Maximum allowed transverse offset versus minimum BOI efficiency:(a) d = 0.05mm, (b) d = 0.2mm, (c) d = 0.4mm. The spot size s = 0.1 mm for all three curves [1]

to, η

$$P_\xi(\eta) = \frac{1}{\sigma_{x\sqrt{2\Pi}}} \int_{\xi^-}^{\xi^+} exp\left[\frac{-x^2}{2\sigma_x^2}\right] dx \tag{2.5}$$

Often,the magnitude of ξ^- and ξ^+ are equal .Thus Equation 2.5 can be written as

$$P_\xi(\eta) = \frac{2}{\sigma_{x\sqrt{2\Pi}}} \int_{0}^{\xi^+} exp\left[\frac{-x^2}{2\sigma_x^2}\right] dx \tag{2.6}$$

The right-hand side of the Equation 2.9 can be put in the form of error function .Thus, the probability can be written as

$$P_\xi(\eta) = erf\left(\frac{\xi^+(\eta)}{\sqrt{\sigma_\xi 2}}\right) \tag{2.7}$$

For a given value of $\xi^+(\eta)$, as σ_ξ decreases the error function tends towards the value of one. This indicates that as the OCM of the BOI is increased, the probability of

aligning the BOI (so that is has a given efficiency)also increases.

The probability of Equation 2.9 is plotted as a function of efficiency in Figure 2.4. The three different curves illustrate the effect of changing the standard deviation in Equation 2.9. We see that as the OCM increases, the standard deviation decreases, the probability increases. Also, we note that for a given standard OCM / standard deviation, as the efficiency increases the probability decreases due to decreasing offsets.

2.3 General BOI alignability

From the previous discussion, we see that if the efficiency of a BOI is relatively insensitive to offset, $\xi^{+}(\eta)$ is large for most values of η (Figure 2.3), then $P_{\xi}(\eta)$ will be higher for most values of η (Figure 2.4). Along with the high $P_{\xi}(\eta)$ value, it seems intuitively,

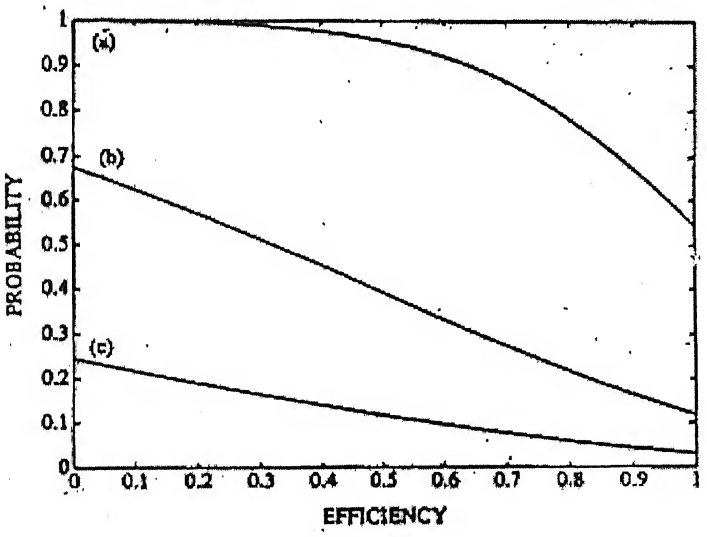

Figure 2.4: Probability versus efficiency: (a) σ = 0.08 mm, (b) σ = 0.2 mm and, (c) σ = 0.4 mm [1]

that the BOI is relatively easy to align; since large offsets are tolerable. Similarly, if the offset must be kept small for good efficiency, then intuitively, the BOI will more difficult to align and $P_\xi(\eta)$ will be low for large range of η values (Figure 2.4a). Based on the correlation between $P_\xi(\eta)$ and our intuitive feel for the ease/difficulty of alignment, we see that the area under the probability versus η curve (Figure 2.4) gives an indication of how easy the BOI is to align. Using this observation, we define the alignability for a given offset, as the area under the $P_\xi(\eta)$ versus η curve. If the offset is very small it could be shown that value of probability for each offset is statistically independent. To include all of the offsets, we can use the product of the individual probabilities and obtain the total BOI alignability A as

$$A = \int_0^1 (P_{l,s}(\eta)P_{t,s}(\eta)P_{a,s}(\eta)P_{l,d}(\eta)P_{t,d}(\eta)P_{a,d}(\eta))\,d\eta \tag{2.8}$$

where the six probabilities, $(P_{l,s}(\eta), P_{t,s}(\eta), P_{a,s}(\eta), P_{l,d}(\eta), P_{t,d}(\eta)$ and $P_{a,d}(\eta)$ arise because both the source and device can have all three offsets : longitudinal, transverse, and angular. In our notation, the subscripts l, t, a, s, and d refer to the words longitudinal, transverse, angular, source, and device, respectively. For example, $P_{l,s}$ is the probability when the BOI has longitudinal offsets of the source.

A depends directly on the parameters of the BOI *ie*

$$A = A(s, d, \lambda, \beta, \theta, x, y, \Delta z, z). \tag{2.9}$$

The alignability A also depends on the OCM. The dependence is due to a change in the σ's, rather than a change in the tolerance to offset, as the OCM is changed. In

either case, changing σ's or changing offset tolerance, $P_\xi(\eta)$ is increased.

The discussion up to this point has been for a single BOI. To find the alignability of a complex interconnect, the interconnect is modeled as a number of BOIs which are connected in series and/or parallel; assuming the probabilities $P_\xi(\eta)$, are independent for the various ξ offset. Then we define the interconnect alignability as the product of the BOI alignability.

The alignability measure A satisfies the limits $0 < A < 1$, The closer A is to unity, the better the alignment of the BOI.

2.4 Alignability of the uniform-uniform BOI

We now have a general definition of alignability. In order to obtain equation into which we can insert numbers and calculate the values, we need to develop BOI efficiency equation, and use the results to integrate the pdfs of the offsets. This section detail this procedure for a typical BOI setup. The assumption taken for the BOI are as follows,

1. The BOI consists of a collimated beam which has a constant intensity value throughout its cross-sectional area and a device which has a constant responsivity across its active area.

2. The shape of the beam and device is square in nature with a side of s and d respectively.

3. value of d is greater than value of s.

From the definition, it should be obvious that the efficiency of the uniform-uniform BOI is simply equal to the area of overlap of the beam and active area of device

2.4.1 Longitudinal offset

A longitudinal offset occurs when the separation between the beam and the device is different than its intended value. This will results in change in the spot size at the device location due to diffractive spreading of the beam. As shown in Figure 2.5, source and device offset (Δ_s & Δ_d respectively) reduce the source device separation (for positive Δ_s or negative Δ_d), will results in smaller spot size. When the offset is in the opposite direction results in larger spot size.

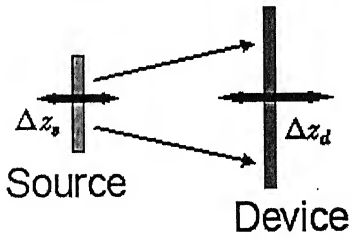

Figure 2.5: Longitudinal offset in BOI

$$\begin{aligned} \eta &= \frac{d^2}{s^2(\Delta z)}, \quad d \leq s(\Delta z) \\ &= 1, \qquad\quad d \geq s(\Delta z) \end{aligned} \tag{2.10}$$

Where $s(\Delta z)$ is offset dependent beam size. The minimum spot size is denoted by s_0, here the maximum efficiency (η_{max}) is 1. Minimum spot size s_0 occurs at source. The intended value of separation is z, the device size at device without any offset is

$$s = s_0 + 2z \tan\beta \tag{2.11}$$

where β is beam divergence.

2.4.1.1 Longitudinal offset in device

If device is shifted by Δz, the spot size at the device become

$$s = s_0 + (2\Delta z) \tan\beta \tag{2.12}$$

By substituting Equation 2.11 in to Equation 2.10 and inverting, we obtained the maximum allowed longitudinal offset for an efficiency η as

$$\Delta z_\eta = \frac{1}{tan(\beta)}(d/\sqrt{\eta} - s_0) - z, \qquad \eta \leq \eta_{max} \tag{2.13}$$

Δz_η indicate the maximum separation between source and device for which efficiency $\geq \eta$. This gives the upper limit of integration while the lower limit is fixed at the value which put the detector directly against the source at $-z$. From the Figure 2.6, it can be observed that

$$\eta = 1, \qquad \Delta z \leq \frac{d-s}{2\tan\beta} \tag{2.14}$$

$$= \frac{d^2}{s(\Delta z)^2}, \qquad otherwise \tag{2.15}$$

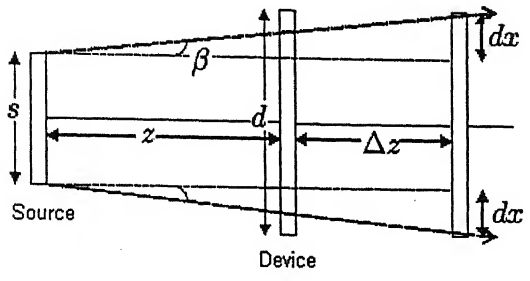

Figure 2.6: Longitudinal offset in BOI

If $\Delta z'$ is the value of offset for which efficiency of BOI is η', then value of probability that efficiency greater than η' ($P(\eta \geq \eta')$) is equal to probability that offset is less than $\Delta z'$ ($P(\Delta z' \leq \Delta z)$). Here we write $P(\eta \geq \eta')$ as $P(\eta')$

$$\begin{aligned} P(\eta') &= \frac{1}{\sigma_l\sqrt{2\pi}} \int_{-z}^{\Delta z'(\eta')} exp\left[\frac{-r^2}{2\sigma_l^2}\right] dx \\ &= \frac{1}{2}\left[erf\left(\frac{z}{\sigma_l\sqrt{2}}\right) + erf\left(\frac{z'(\eta')}{\sigma_l\sqrt{2}}\right)\right], for\ \Delta z \geq 0 \\ &= \frac{1}{2}\left[erf\left(\frac{z}{\sigma_l\sqrt{2}}\right) - erf\left(\frac{z'(\eta')}{\sigma_l\sqrt{2}}\right)\right], for\ \Delta z \leq 0 \end{aligned} \tag{2.16}$$

Using Equation 2.16 and Equation 2.10 we can get plot between probability versus longitudinal offset and efficiency versus longitudinal offset respectively, hence variation of probability versus efficiency could also be drawn as shown in Figure 2.7. Area under this curve gives the value of alignability.

2.4.1.2 Longitudinal offset in source

For source offset, the sign of limit in integration given by Equation 2.16 would need to be inverted. However because of the symmetry of the equation this is not really necessary. For either case probability will be same and given by Equation 2.16

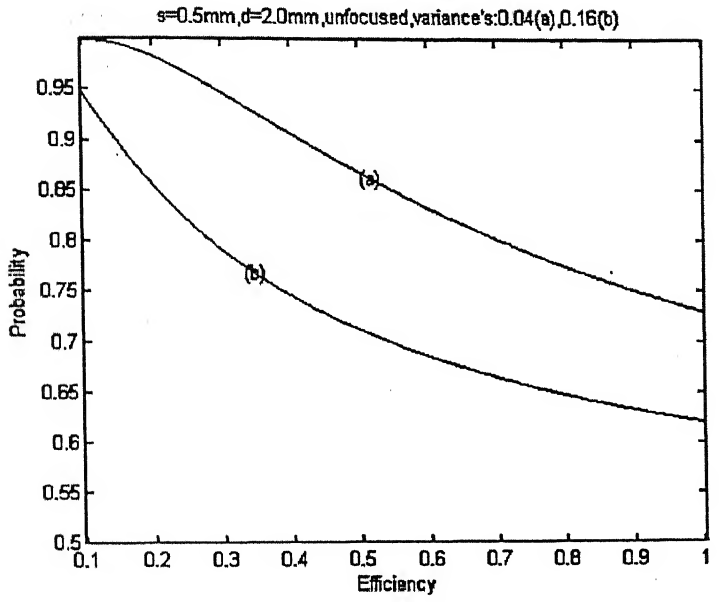

Figure 2.7: Probability versus efficiency curve for longitudinal offset in BOI

Analyzing the probability versus efficiency curve for different value of offset illustrated by Figure 2.7, as the value of standard deviation increases, area under the curve *i.e.* value of alignability decreases.

Figure 2.8 illustrates the alignability vs normalized device size curve. With the increase of normalized device size alignability value is also increasing.

2.4.2 Transverse offset

When the beam front and the surface of the device are parallel but not concentric, the BOI has a transverse offset, as illustrated in Figure 2.9. In general, this offset has two components, x and y, but in our case we are assuming that there exist only one offset along x direction.

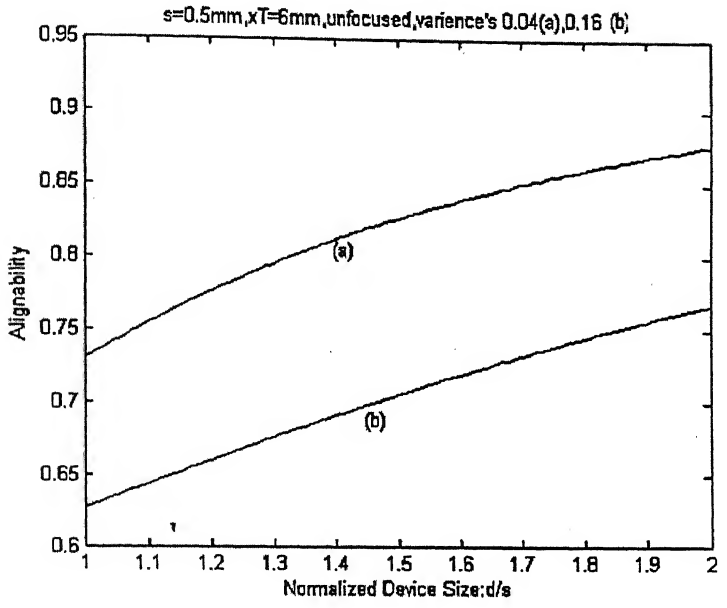

Figure 2.8: Alignability versus normalized device size for longitudinal offset in BOI

2.4.2.1 Transverse offset in Device

We have assumed that the value of device is larger than spot, $d \geq s$, then the nominal efficiency, $\eta_{nom} = 1$, this efficiency will remain at this value until the offset is large enough to shift the device partially out of the beam. If r denotes the offset in x direction, it can be shown that the efficiency for different range of offset r is given by,

$$\begin{aligned} \eta &= 0, && |r| \geq \left(\frac{d+s}{2}\right) \\ &= 1, && |r| \leq \left(\frac{d-s}{2}\right) \\ &= 1/s(d/2+s/2-x), && -\left(\frac{d+s}{2}\right) \leq r \leq -\left(\frac{d-s}{2}\right) \\ & && and \left(\frac{d-s}{2}\right) \leq r \leq \left(\frac{d+s}{2}\right) \end{aligned} \tag{2.17}$$

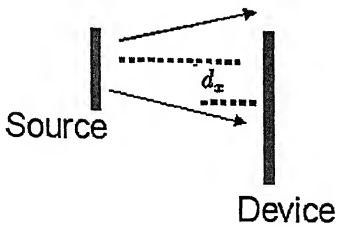

Figure 2.9: Transverse offset

pdf of transverse offset is given by,

$$f_r(r) = \frac{1}{\sigma_r\sqrt{2\pi}}\ exp\left[\frac{-r^2}{2\sigma_r^2}\right] \tag{2.18}$$

where σ_r denotes the standard deviation of the offset and r denotes the value of the offset. Using Equation 2.18, we can plot the graph of probability versus offset.

If $\pm r$ is the value of offset for which efficiency of BOI is η', then value of probability that efficiency greater than η' ($P_{ts}(\eta \geq \eta')$) is equal to probability that offset is less than $\pm r'$. We write $P_{ts}(\eta \geq \eta')$ as $P_{ts}(\eta')$, given by Equation 2.19

$$\begin{aligned} P(\eta_{ts}) &= \frac{1}{\sigma_t\sqrt{2\pi}}\int_{-r'}^{r'} exp\left(\frac{-r^2}{2\sigma_t^2}\right) dr \\ &= erf\left(\frac{r}{\sqrt{2\sigma_t}}\right) \end{aligned} \tag{2.19}$$

Using Equation 2.18 and Equation 2.19 we can get plot between probability versus efficiency and the value of alignability. Plot for probability versus efficiency is illustrated in Figure 2.10 for different values of σ_t. Alignability variation with normalized device size is shown in Figure 2.11.

Also in case of transverse offset because of symmetry of BOI, the alinability value

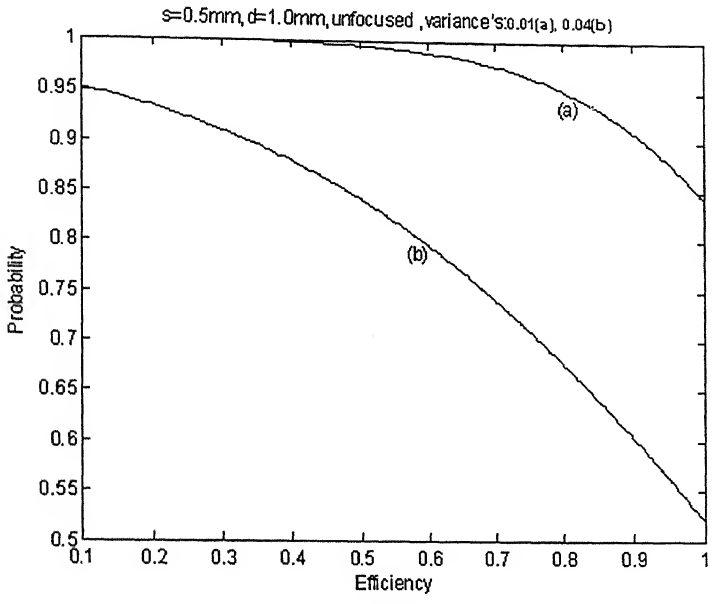

Figure 2.10: Probability versus efficiency plot for transverse offset in BOI

will remain same for source and device offsets.

2.4.3 Angular offset

An angular offset occurs when the source (direction of beam propagation) or device are titled with respect to BOI optical axis. In Figure 2.12(a) we see an angular offset in device. This type of offset results in the effective change in the area of the device and shape become rectangular with side as d and $d\cos\theta$. For angular offset in source, as shown in Figure 2.12(b) beam also has an effective area and shape change. However there is also an induced transverse offset dx. This difference requires that efficiency and probability calculation be handled differently for source offset than device offset. For simplification we have considered angular offset only along x direction. From the

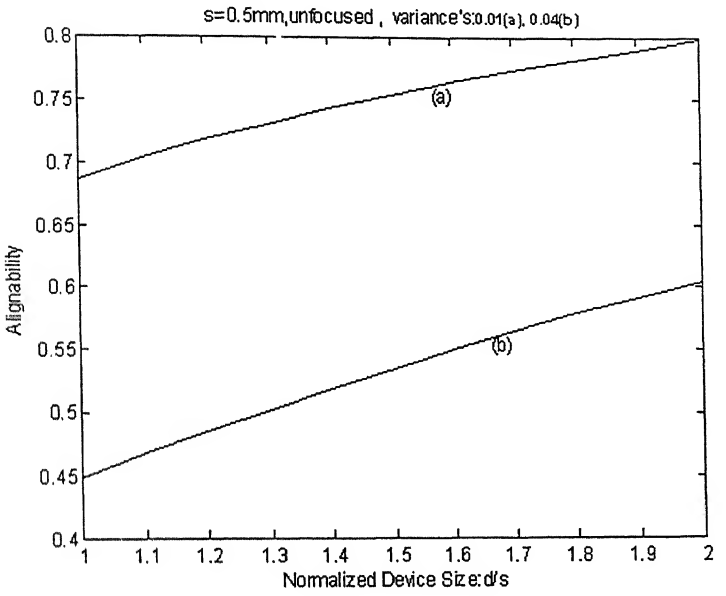

Figure 2.11: Alignability versus normalized device size plot for transverse offset in BOI

Figure 2.13, we can write the relation between efficiency and angular offset in device, and is given by Equation 2.20. pdf of angular offset is given by Equation 2.21.

$$\begin{aligned} P(\eta_{ad}) &= 1, & 0 \leq \theta \leq \theta_c \\ &= \frac{sd\cos\theta}{s^2}, & \theta_c \leq \theta \leq \theta_m \end{aligned} \tag{2.20}$$

pdf of angular offset is given by Equation 2.21.

$$f_\theta = \frac{1}{\sigma_\theta \sqrt{2\pi}} exp\left[\frac{-\theta^2}{2\sigma_\theta^2}\right] \tag{2.21}$$

where σ_θ denotes the standard deviation of the offset and θ denotes the value of the offset. Using Equation 2.21, we can plot the graph of probability versus offset. Using Equation 2.20 and Equation 2.21, we can get the plot of probability versus efficiency,

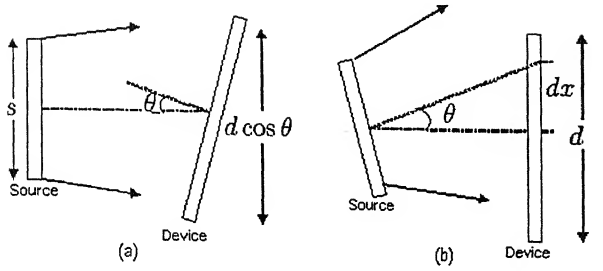

Figure 2.12: Illustration of the difference between angular offset of the device (a) and source (b)

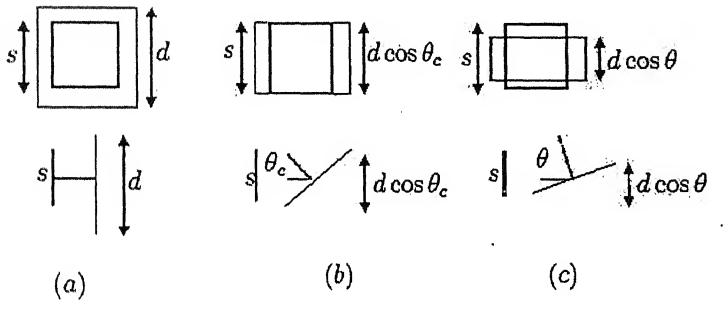

Figure 2.13: Various overlap positions of the BOI with angular offset in device (a) $\theta = 0$, (b) $\theta = \theta_c$, and (c) $\theta = \theta$

illustrated in Figure 2.15.

2.4.3.1 Angular offset in source

Now that we have determine the efficiency and probability expression for angular offset of the device, we need to do the same for angular offset of the source. As mentioned previously, there will be now an induced transverse offset which shifts the center of beam away from the center of the device. The induced transverse offset is given by

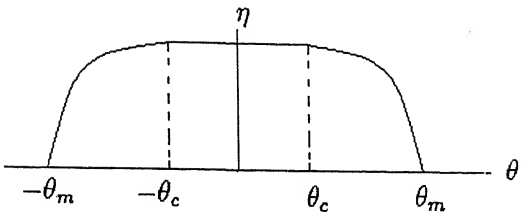

Figure 2.14: Efficiency verses angular offset in device

$dx = z\tan(\theta)$, Because we have assumed that device is larger than spot size of beam at device, without any offset the efficiency will be equal to maximum efficiency, (η_{max}) = 1, up to the point at which the edge of beam is touching the edge of the device. At this point, $dx + s'/2 = d/2$, Where $s' = s/\cos\theta$. This equation can be written as,

$$z\tan(\theta_c) + \frac{s}{2\cos\theta_c} = \frac{d}{2}$$

$$\theta_c = \sin^{-1}\left(\frac{d}{\sqrt{d^2+(2z)^2}}\right) - \sin^{-1}\left(\frac{s}{\sqrt{d^2+(2z)^2}}\right) \tag{2.22}$$

Referring to Figure 2.16, we can write the relation between efficiency and angular offset as,

$$\begin{aligned} \eta &= 1, && \theta \le \theta_c \\ &= (dx + d/2 + s/2\cos\theta)\, s/s^2, && \theta_c < \theta \le \theta_m \\ &= 0, && otherwise \end{aligned} \tag{2.23}$$

Where θ_m is the offset at which the efficiency became zero. Using the above relations we can plot the graph between probability versus efficiency as illustrated in Figure 2.17.

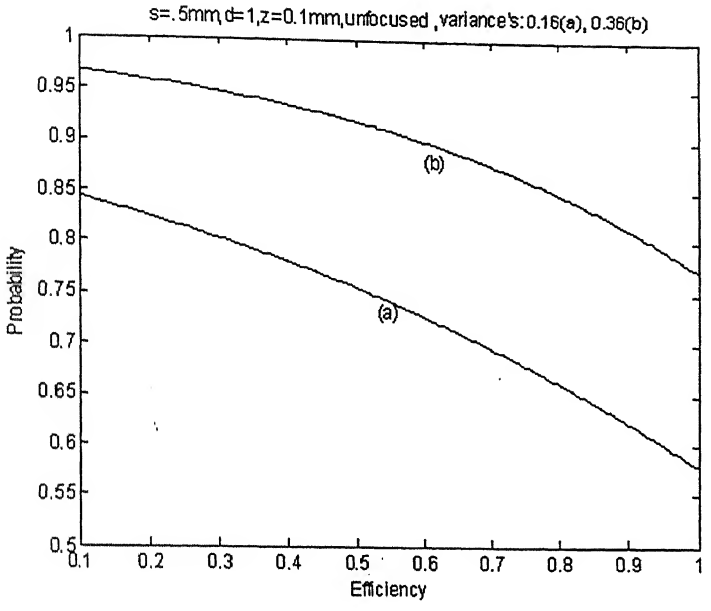

Figure 2.15: Probability versus efficiency plot for angular offset in the device

2.5 Observation

Analyzing the probability versus efficiency curves for different values of the variance of the pdf of offset, it can be deduce that as the the value of variance increases, area under the probability versus efficiency curves *i.e.* alignability value decreases. These results support our intuition about the relation of alignability and variance of pdf of the offset. Also the plots of alignability and normalized device size illustrate that as the ratio of device size and beam size increases the alignability value increase gradually *i.e.* for higher ratio of device size and beam size aligning the BOI is easy, which is true. These results suggest that higher the value of alignability indicates easy to align the BOI.

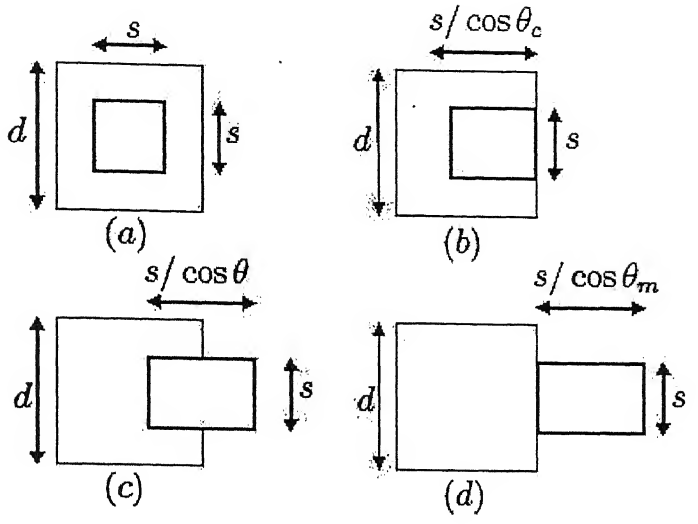

Figure 2.16: Various overlap positions for a BOI with angular offset in device (a)$\theta = 0$, (b)$\theta = \theta = \theta_c$, (c)$\theta < \theta_c < \theta_m$, (d) $\theta \geq \theta_m$

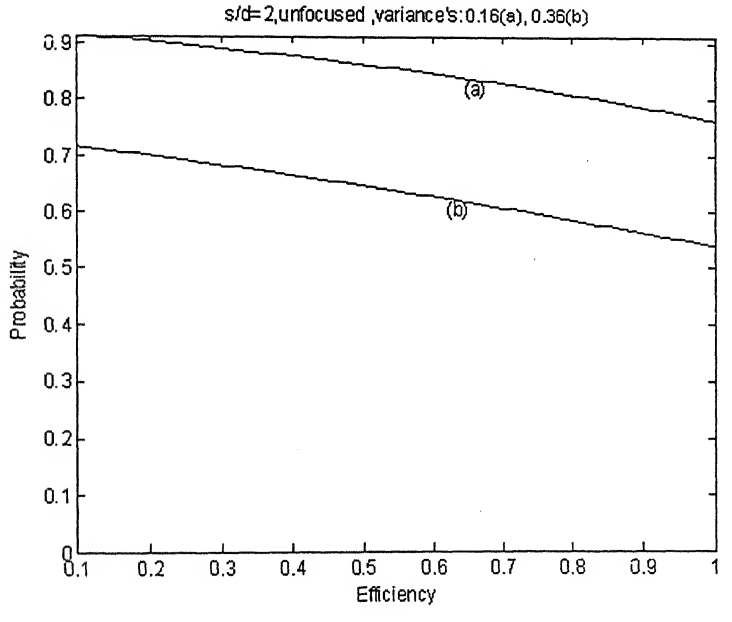

Figure 2.17: Probability versus efficiency plot for angular offset in the source

Chapter 3

Background Theory

This chapter will illustrates the theories that are necessary to support the analysis in this thesis paper.

3.1 Diffraction theory

Referring the Figure 3.1, the field distribution from a source is observed on a screen. The field distribution on the screen is called diffraction pattern[2]. Let $E(x_i, y_i)$ rep-

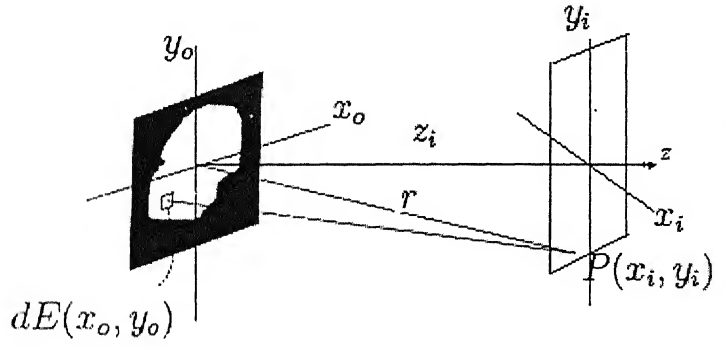

Figure 3.1: Diffraction pattern

resents the field at P on the screen placed at a distance z_i away from the source field $E(x_o, y_o)$. The distributed source $E(x_o, y_o)$ is considered as an ensemble of the point sources. Each points source radiates a spherical wave. The field at the observation point P is comprised of contribution from an ensemble of field radiated from all the points sources. The contribution of the points source located at (x_o, y_o) to the point P at (x_i, y_i) is

$$dE(x_i, y_i) = \frac{e^{jkr}}{r} E(x_o, y_o) dx_o dy_o \tag{3.1}$$

where $E(x_o, y_o)$ is the magnitude of the point source located at (x_o, y_o) and r is the distance between (x_o, y_o) and (x_i, y_i). The distance r is expressed as

$$r = \sqrt{z_i^2 + (x_i - x_o)^2 + (y_i - y_o)^2} \tag{3.2}$$

The contribution of the spherical waves from all the point source to $E(x_i, y_i)$ is

$$E(x_i, y_i) = k \int\int \frac{e^{jkr}}{r} E(x_o, y_o) dx_o dy_o \tag{3.3}$$

This equation is known as the Fresnel-Kirchhoff diffraction formula. The amplitude of the diffracted field is inversely proportional to the wavelength and is expressed as

$$k = \frac{1}{j\lambda} \tag{3.4}$$

If the point of observation is far enough away or in the vicinity of z axis (paraxial),

$$z_i^2 \gg (x_i - x_o)^2 + (y_i - y_o)^2 \tag{3.5}$$

then the distance r can be simplified by binomial expression as

$$r = z_i \left(1 + \frac{(x_i - x_o)^2 + (y_i - y_o)^2}{2z_i^2}\right) \tag{3.6}$$

which can be rewritten as

$$r \cong z_i + \frac{x_i^2 + y_i^2}{2z_i} - \frac{x_i x_o + y_i y_o}{z_i} + \frac{x_o^2 + y_o^2}{2z_i} \tag{3.7}$$

The region of z_i for which the this approximate expression Equation 3.7 is called the Fresnel region or near-field region. As the distance further increased in the z direction, the last term in Equation 3.7 became negligible for the finite size of the source. This region of z_i is called Fraunhofer region or far-field region. In the far-field region the, the approximation for r is

$$r = z_i + \frac{x_i^2 + y_i^2}{2z_i} - \frac{x_i x_o + y_i y_o}{z_i} \tag{3.8}$$

By substituting this expression into the exponential term of Fresnel-Kirchhoff diffraction formula, Equation 3.3, the field becomes

$$E(x_i, y_i) = \frac{1}{jk\lambda} e^{jk(z_i + \frac{x_i^2 + y_i^2}{2z_i})} \int\int_{-\infty}^{\infty} E(x_o, y_o) e^{-j2\pi(f_x x_o + f_y y_o)} dx_o dy_o$$
$$with f_x = \frac{x_i}{\lambda z_i}, f_y = \frac{y_i}{\lambda z_i} \tag{3.9}$$

We recognize that the integral is the two-dimensional Fourier transform of the field in the x, y domain in to the f_x, f_y domain. It can also be represented as

$$E(x_i, y_i) = \frac{1}{jk\lambda} e^{jk(z_i + \frac{x_i^2 + y_i^2}{2z_i})} F\{E(x_o, y_o)\}_{f_x = \frac{x_i}{\lambda z_i}, f_y = \frac{y_i}{\lambda z_i}} \tag{3.10}$$

where F denotes the Fourier transform. In short, the Fraunhofer diffraction pattern is the Fourier transform of the source field.

In case of near field or Fresnel diffraction, as discussed substituting the value of r from Equation 3.7 into Fresnel-Kirchhoff diffraction formula, Equation 3.3, the result is

$$E(x_i, y_i) = \frac{j}{k\lambda} e^{z_i + \frac{x_i^2 + y_i^2}{2z_i}} \int\int_{-\infty}^{\infty} E(x_o, y_o) e^{jk\frac{(x_o^2 + y_o^2)}{2z_i}} e^{-j2\pi(f_x x_o + f_y y_o)} dx_o dy_o$$

$$with f_x = \frac{x_i}{\lambda z_i}, f_y = \frac{y_i}{\lambda z_i} \qquad (3.11)$$

3.2 A thin lens as a phase transformer

A lens is composed of optically dense material, usually glass, in which the propagation velocity of an optical disturbance is less than velocity in air. A lens is said to be *thin lens* if a ray entering at coordinates (x, y) on one face emerges at approximately the same coordinates on the opposite face, *i.e.*, if there is negligible translation of the ray within the lens. Thus a thin lens simply delay [3] an incident wavefront by an amount proportional to the thickness of the lens at each point.

Referring to the Figure 3.2, if the complex field $U'_{l(x,y)}$ across a plane immediately behind the lens is related to complex field $U_{l(x,y)}$ incident on a plane immediately in front of the lens by

$$U'_{l(x,y)} = t_l(x, y) U_{l(x,y)} \qquad (3.12)$$

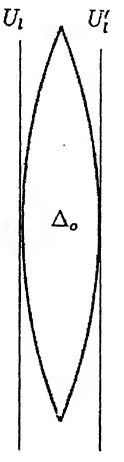

Figure 3.2: Thin lens

where $t_l(x,y)$ can be calculated for thin lens as

$$t_l(x,y) = exp\,[jkn\triangle_0]\ exp\Big[-j\frac{k}{2f}(x^2+y^2)\Big]P(x,y) \tag{3.13}$$

The factor $P(x,y)$ is multiplied to take the finite aperture of lens into consideration. $P(x,y)$ is given by

$$P(x,y) = \begin{cases} 1 & \text{inside the lens aperture} \\ 0 & \text{otherwise} \end{cases}$$

3.3 Beam propagation method

The motive of the thesis is to estimate the alignability value for a practical optical interconnect. For finding the alignability(discussed in detail in next chapter) we require an optical beam propagation technique that is computationally fast, supports diffractive effects, and is valid for the small sizes and propagation distances of the optical

MEM components and systems.

Ray, or geometric, optics are the simplest of the optical propagation methods. This method traces rays of light through refractive elements, however has no inherent support for the optical characteristics of light. This is improved by using Gaussian optics, which satisfies the paraxial Helmholtz equation in solving for optical parameters such as waist size, depth of focus, intensity, and phase, meeting the optical criteria which is required for modeling optical MEM systems. An additional benefit of using Gaussian analysis is that we can approximate the behavior of the lasers used in these systems as sources of Gaussian shaped beams. The greatest advantage of both these methods is speed. Using nine scalar parameters to define a Gaussian beam and the ABCD matrix equations for optical interfaces, no explicit integration is needed to calculate the resulting Gaussian beam at the interface to adjacent components.Mostly commercially available software are using these techniques for modeling optical beam propagation.

However the interconnect we have the effect of truncation of beam due to small aperture of optical component is noticeable and in above two method, it has been assumed that the size of optical component is large enough relative to the beam size so the truncation of beam is negligible. Therefore we need to consider appropriate optical propagation methods which can meet this objective without sacrificing simulation speed.

All scalar diffraction solutions are limited by two assumptions [4]; the diffracting

structures must be "large" compared with the wavelength of the light and the observation screen can not be "too close" to the diffracting structure. The concept of "too close" is defined for each approximation model in Figure 3.3. This figure shows light passing through an aperture plane (ξ, η), propagating a distance z past the aperture, and striking an observation plane (x, y). The figure also presents equations calculating the validity of the diffractive models with respect to the distance propagated past the aperture, in terms of the limits of the aperture and observation planes, the wavelength of light,λ, and the wave number, $k = \frac{2\pi}{\lambda}$.

Working from the right to left of Figure 3.3, we first investigate the least accurate

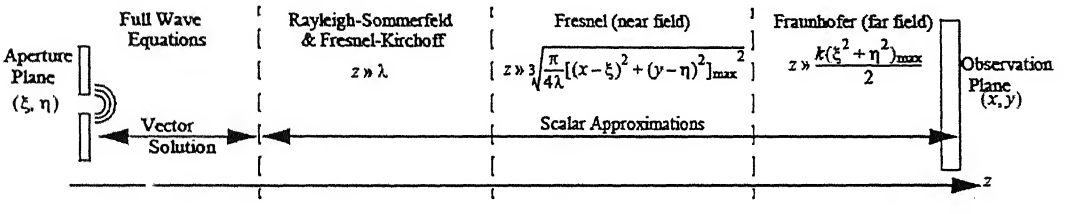

Figure 3.3: Optical Propagation Distance, z, Aperture Size, (ξ, η), Observation Plane Size, (x, y)[4]

of the scalar approximations, the Fraunhofer approximation. The advantage of this technique is the ability to implement a Fourier transform to solve the complex wave function. The Fraunhofer technique is valid when the light striking the aperture plane can be assumed to be a plane wave. Most diffractive software tools perform Fraunhofer propagation, using a common FFT routine for quick evaluation. As shown in Figure 3.3, the Fraunhofer approximation is valid in the "far-field", where the light has propagated

to a distance far from the aperture, and the diffraction pattern is essentially the same as that at infinity. However, for most optical MEM systems like our optical interconnect, the far field is not of concern.

To illustrate the problem of this method with respect to optical interconnect we are analyzing, using the equation found in Figure 3.3, the minimum propagation distance for the Fraunhofer approximation to be valid is $26361\mu m$, which is much higher then the propagation distance we are considering for optical interconnect.

To remove the plane-wave limitation of the far-field, our study moves towards more rigorous optical models. We next examine the Fresnel approximation, valid in both the far and near field. The "near field" is defined as the region closer to an aperture where the diffraction pattern differs from that observed at an infinite distance. No longer can a fast Fourier transform be used for this calculation, as the light hitting the aperture plane is no longer a plane wave and an explicit integration of the wave front must be calculated. When solving for the minimum propagation distance for validity with the same optical interconnect system as before, we find the propagated distance must be larger than $700\mu m$, which is near to propagation distance we have taken for the optical interconnect, so we have used Fresnel near field approximation for calculating the diffraction.

Chapter 4

Practical Optical Interconnect Analysis

In a practical optical interconnect we use laser as source of light. Intensity profile of laser beam can be approximated as gaussian. The effect of a lens on a Gaussian beam using the complex beam parameter has been discussed in many text books, but this method does not take into consideration the finite size of lens aperture and it is assumed that the beam propagates without any change .When the aperture of a lens is of the same order as the beam width (spot size) the diffraction phenomena becomes noticeable because of truncation effect of finite size of optical components, and the field is different form that obtained by the complex beam parameter method. So for the propagation of beam we will not consider the simple ABCD matrix analysis or any other method in which aperture size is assumed to be infinite.

In the analysis of optical interconnect, we have divided the total propagation of beam in to four parts, the amplitude distribution at different part of optical intercon-

nect is illustrated in Figure 4.1.

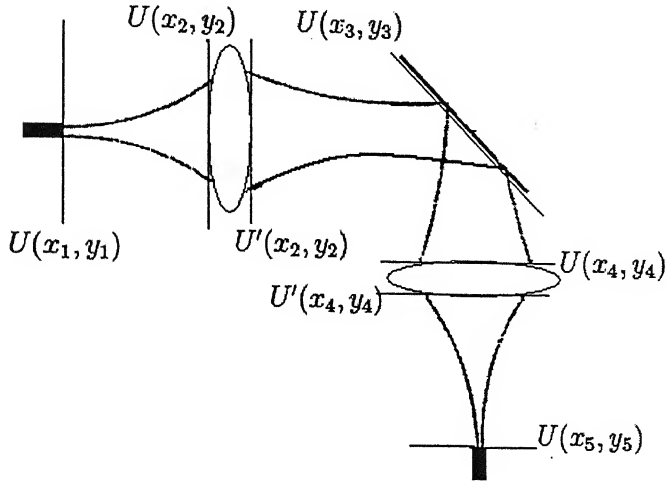

Figure 4.1: Amplitude distribution at different positions of optical interconnect

1. Source to first lens

2. First lens to the mirror

3. Mirror to the second lens

4. Second lens to detector

4.1 Source to first lens

We assumed that the intensity profile of laser light from the source is gaussian in nature, the distribution of Gaussian beam is $U(x_1, y_1)$ at the source is given by Equation 4.1,

$$U(x_1, y_1, z_1) = A\left\{\frac{w_0}{w(z)} exp\left[-\frac{r^2}{w_z^2}\right]\right\} \times exp\left\{-j\left[kz - \arctan\frac{z}{z_0}\right]\right\} \times exp\left[-j\frac{kr^2}{2R(z)}\right] \tag{4.1}$$

where z is propagation direction of Gaussian beam,

$r=\sqrt{x^2+y^2}$ is Distance from the axis of the Gaussian beam,

k is $\frac{2\pi}{\lambda}$and

w_0 is 1/e half-width at beam waist.

z_0 is the parameter defined as

$$z_0 = \pi w_0^2/\lambda \tag{4.2}$$

for free space. The divergence of the optical beam results in an increase of the $1/e$ half-width w_z with z is given by

$$w_z = w_o\sqrt{1+\left(\frac{z}{z_0}\right)^2} \tag{4.3}$$

and yields a curved wave-front whose radius is represented by

$$R_z = z\left[1+\left(\frac{z_0}{z}\right)^2\right] \tag{4.4}$$

as the gaussian beam propagates from source to first lens the because there is no truncation in the path the beam profile remain gaussian, only there will be change in phase and beam width. Assume that the amplitude distribution just before the lens in $U(x_2, y_2)$.

4.2 First lens to mirror

The lens is a converging lens of focal length f_1, The finite extent of the lens aperture can be accounted for by associating with the lens a pupil function $P_{f_1}(x_2, y_2)$ defined by

$$P_{f_1}(x_2, y_2) = \begin{cases} 1 & \text{inside the lens aperture} \\ 0 & \text{otherwise} \end{cases}$$

as the beam pass through the lens we have to multiply the amplitude distribution with the lens transformation factor which is given by,

$$U_l'(x, y) = U_l(x, y)\ exp\,[jkn\triangle_0]\ exp\Big[-j\frac{k}{2f}(x^2 + y^2)\Big] \tag{4.5}$$

The first term is simply a constant phase delay, while the second term we may interpret as a quadratic approximation to a spherical wave. If the focal length is positive, then the spherical wave is converging toward a point on the lens axis a distance f behind the lens. If f is negative, then the wave is diverging about a point on the lens axis a distance f in front of the lens. However we have converging lens, thus the amplitude distribution just behind the lens became

$$U'(x_2, y_2) = U(x_2, y_2)P(x_2, y_2)\ exp\Big[-j\frac{k}{2f}(x_2^2 + y_2^2)\Big] \tag{4.6}$$

The constant phase delay associated with the lens transformation has been omitted since it does not affect the result in any significant way. The factor $P(x_2, y_2)$ is multiplied to take the finite aperture of lens into consideration.

To find the distribution $U(x_3, y_3)$ of field amplitude behind the lens at any distance z, using the Fresnel formula as given by Equation 3.11 we can find the distribution at

a distance z from the first lens as,

$$U(x_3,y_3) = \frac{exp(jkz)}{jkz}\, exp\Big[-j\frac{k}{2z}(x_3^2+y_3^2)\Big]\int\int_{-\infty}^{\infty} U'(x_2,y_2) \\ exp\Big[j\frac{k}{2z}(x_2^2+y_2^2)\Big]exp\Big[-j\frac{2\pi}{\lambda z}(x_2x_3+y_2y_3)\Big]dx_2dy_2 \qquad (4.7)$$

substituting equation 4.6 in to equation 4.7,

$$U(x_3,y_3) = \frac{exp(jkz)}{jkz}\, exp\Big[-j\frac{k}{2z}(x_3^2+y_3^2)\Big]\int\int_{-\infty}^{\infty} U(x_2,y_2) \\ P(x_2,y_2)\, exp\Big[-j\frac{k}{2f}(x_2^2+y_2^2)\Big]exp\Big[j\frac{k}{2z}(x_2^2+y_2^2)\Big] \\ exp\Big[-j\frac{2\pi}{\lambda z}(x_2x_3+y_2y_3)\Big]dx_2dy_2 \qquad (4.8)$$

so the equation 4.8, indicate the amplitude distribution at the mirror which is kept at a z distance from the first lens.

4.3 Mirror to second lens

The mirror is perfectly aligned so that after reflection from mirror the beam will incident directly on the second lens. For finding the amplitude distribution on the second lens again we have to apply Fresnel formula as Equation 3.11. If the amplitude distribution at mirror is denoted by $U(x_3,y_3)$ so amplitude distribution at the second lens is given by $U(x_4,y_4)$ as,

$$U(x_4,y_4) = \frac{exp(jkz)}{jkz}\, exp\Big[-j\frac{k}{2f}(x_4^2+y_4^2)\Big]\int\int_{-\infty}^{\infty} U(x_3,y_3)P_m(x_3,y_3) \\ exp\Big[j\frac{k}{2z}(x_3^2+y_3^2)\Big]exp\Big[-j\frac{2\pi}{\lambda z}(x_3x_4+y_3y_4)\Big]dx_3dy_3 \qquad (4.9)$$

where $P_m(x_3, y_3)$ is pupil function of mirror because of its finite size, which is defined as,

$$P_m(x_3, y_3) = \begin{cases} 1 \text{ inside the mirror aperture} \\ 0 \text{ otherwise} \end{cases}$$

substituting the value of $P_m(x_3, y_3)$ and $U(x_3, y_3)$ in equation 4.9 we can get the amplitude distribution $U(x_4, y_4)$ at the second lens.

4.4 Second lens to the detector

After passing through the second lens the beam will finally fall on the detector. So finding the amplitude distribution on the detector we again have to use the Fresnel formula as indicated by Equation 3.11. Just before the second lens the amplitude distribution is given by $U(x_4, y_4)$ so just beyond the second lens the amplitude distribution will given by,

$$U'(x_4, y_4) = U(x_4, y_4)P(x_4, y_4)\ exp\Big[-j\frac{k}{2f_2}(x_2^2 + y_2^2)\Big] \tag{4.10}$$

where $P(x_4, y_4)$ is pupil function of the second lens because of the finite size of the aperture which is defined as,

$$P_{f_2}(x_4, y_4) = \begin{cases} 1 \text{ inside the second lens aperture} \\ 0 \text{ otherwise} \end{cases}$$

and f_2 is focal length of the second lens. Using Fresnel formula, amplitude distribution on the detector $U(x_5, y_5)$ is given by Equation 4.11

$$U(x_5,y_5)=\frac{exp(jkz)}{jkz}\,exp\Big[-j\frac{k}{2z}(x_5^2+y_5^2)\Big]\int\int_{-\infty}^{\infty}U'(x_4,y_4)$$
$$exp\Big[j\frac{k}{2z}(x_4^2+y_4^2)\Big]exp\Big[-j\frac{2\Pi}{\lambda z}(x_4x_5+y_4y_5)\Big]dx_4dy_4 \qquad (4.11)$$

or

$$U(x_5,y_5) = \frac{exp(jkz)}{jkz}\,exp\Big[-j\frac{k}{2z}(x_5^2+y_5^2)\Big]\int\int_{-\infty}^{\infty}U(x_4,y_4)P_{f_2}(x_4,y_4)$$
$$exp\Big[j\frac{k}{2z}(x_4^2+y_4^2)\Big]exp\Big[-j\frac{2\pi}{\lambda z}(x_4x_5+y_4y_5)\Big]dx_4dy_4 \qquad (4.12)$$

by substituting the values of $U(x_4,y_4)$ and $P_{f_2}(x_4,y_4)$ in Equation ?? we can deduce the amplitude distribution on the detector.

4.5 Solving the Integration

We can not get the close form solution of above integrals. For solving it we have to use some numerical integration method. We have used Simpsons method for calculating the integral. We verified the accuracy of the program for integration made in Mathematica by comparing the few known result with the result we get from Simpson method and find the the error is less than 0.08% (Discussed in Appendixes A).

During the integration one issue we always take care that is the issue of spurious results because of aliasing effect. To avoid aliasing the rate of sampling *i.e.* step size for numerical integral very high so that there could no aliasing.

4.6 Power calculation

As shown in last section we can find the amplitude of field distribution at different positions of the optical interconnect. From there we can deduce the intensity distribution as,

$$I(x,y) = U(x,y)U^*(x,y)$$

where $U^*(x,y)$ represent the conjugate of $U(x,y)$, hence we can find the value of power coupled to a particular optical component by integrating the intensity over the limits of size of the that component.

Suppose the component is circular in shape with radius of curvature r, the power coupled to this component will be given by Equation 4.13,

$$P = \int_{-r}^{r} \int_{-\sqrt{r^2-y^2}}^{\sqrt{r^2-y^2}} I(x,y)dxdy \tag{4.13}$$

In this chapter we estimated the intensity distribution at different positions of the interconnect. By integrating the intensity distribution over the active area of optical components we can calculate the power coupled to the respective component.

Chapter 5

Alignability of practical optical interconnect

For a simple BOI, alignability calculation has been shown in §2.3. It has been assumed that a BOI consists of a collimated beam which has a constant intensity value throughout its cross-sectional area and a device which has a constant responsivity across its active area. This setup is called uniform-uniform BOI.

To begin, we define the BOIs "emitter plane" and "receiving plane" as the planes in which the optical beams are emitted and received, respectively.

The alignability calculation for a practical optical interconnect is similar to the method discussed in §2.3. This chapter extends the alignability definition for a uniform-uniform BOI to a practical optical interconnect. To find the alignability of a complex interconnect the one illustrated in Figure 5.1, the interconnect is modeled as a number of BOIs which are connect in series and/or parallel. The overall alignability of the interconnect is the product of individual BOIs' alignability.

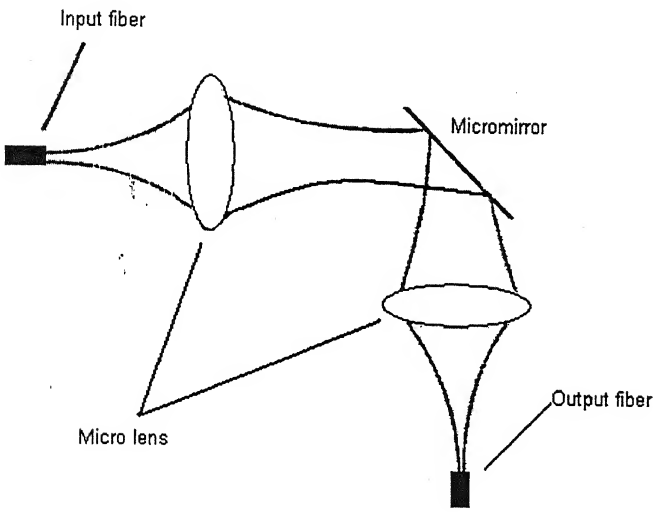

Figure 5.1: Practical optical interconnect

The optical interconnect is divided in 4 BOIs as illustrated in Figure 5.2. The alignability of the whole system is defined as multiplication of the individual alignability of each BOI. In the case of uniform-uniform BOI, the beam is confined in a particular region. In the absence of any offset, maximum power will fall on the device leading to a maximum efficiency. With the introduction of an offset the efficiency starts decreasing and at a certain value of the offset it becomes zero. The probability is now calculated for different values of efficiency starting from the maximum efficiency case to zero efficiency case. The area under the probability versus efficiency curves give the value of alignability. A higher value of the alignability indicate the ease with which an optical interconnect can align.

The assumption that nature of the light beam is gaussian leads to the fact that effi-

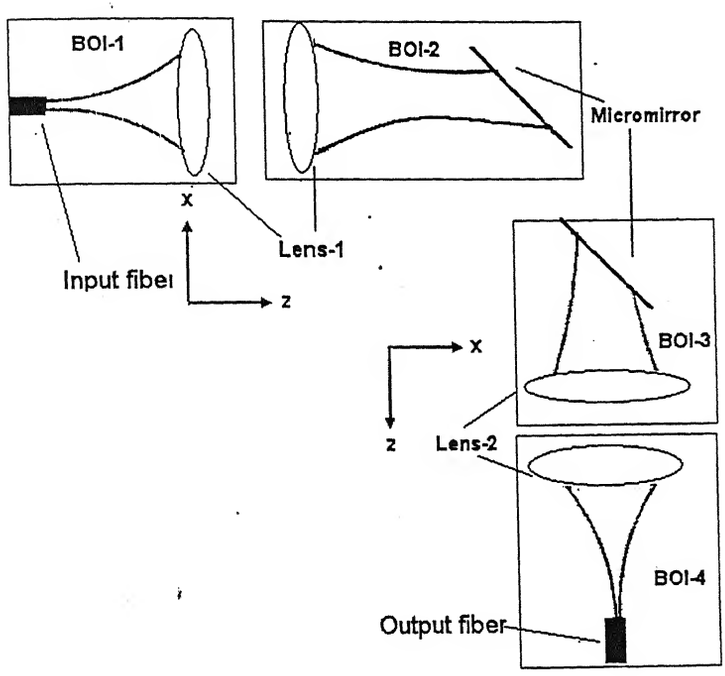

Figure 5.2: Divided practical optical interconnect

ciency can never assume a zero value in spite of maximum offset value. The alignability definition is thus modified by taking only those values of efficiency which are greater that or equal to 0.1. The justification for this definition is due to the consideration that, in a practical interconnect the probability that efficiency will greater that 0.1 will always be very high and reaching to 1, so even if we take take the minimum value of efficiency equal to 0.1 the relative difference in the value of alignability for different setup of practical optical interconnect will not change.

For calculating the alignability of each BOI, we have considered only the following offsets.

For BOI-1, a transverse offset in x-direction has been considered in the lens.

For BOI-2, a transverse offset in x-direction has been considered in the mirror.

For BOI-3, a angular offset along y-direction plane has been considered in the mirror.

For BOI-4, a transverse offset in x-direction has been considered in the detector.

5.1 Alignability of BOI-1

We have assumed that the intensity profile of the laser beam from the source is gaussian. For BOI-1,the beam travels from the source to the first lens as illustrated in Figure 5.2.

The amplitude distribution $U(x_2, y_2)$ on the first lens has been calculated in §4.2. If there is no misalignment the power incident on the lens can be calculated by integrating the intensity distribution over the active area of lens, as given by Equation 4.13. When transverse offset along the x-direction occurs in the first lens, the change in the incident power on the active area of lens can be calculated as,

$$P = \int_{-r}^{r} \int_{k-\sqrt{r^2-y^2}}^{k+\sqrt{r^2-y^2}} I(x,y)dxdy \tag{5.1}$$

where k is the value of transverse offset along x-direction.

The efficiency of BOI-1 can be estimated by Equation 5.2,

$$\eta_{BOI-1} = \frac{Power\ coupled\ to\ the\ first\ lens}{Total\ power\ in\ the\ beam\ from\ the\ source\ for\ BOI-1} \tag{5.2}$$

The total power in the beam from the source for BOI-1 is total power in the gaussian beam emitted by the source. The intensity distribution on the first lens is shown in Figure 5.3 where I_{l_1} is intensity distribution. Using intensity distribution and Equa-

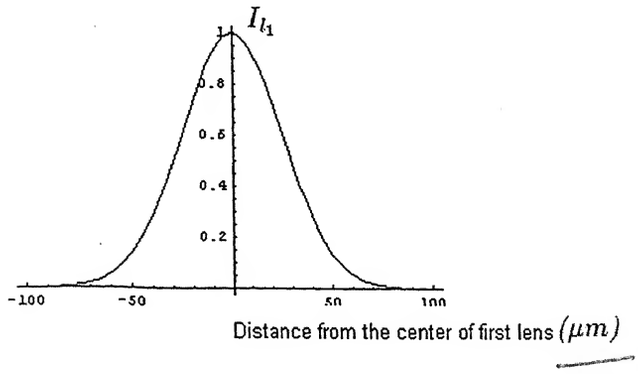

Figure 5.3: Intensity distribution on first lens

tion 5.1 we can find the efficiency values for different offset. The plot of efficiency versus offset is shown in Figure 5.4 We also know that the probability density function

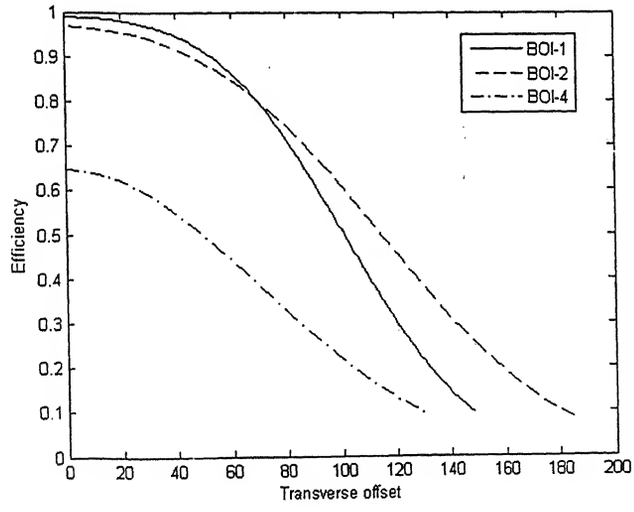

Figure 5.4: Efficiency versus transverse offset (μm) for BOI-1, BOI-2 and BOI-3

of the offset is gaussian in nature as given by Equation 5.3,

$$f_x(x) = \frac{1}{\sigma_x\sqrt{2\pi}}\, exp\left[\frac{-x^2}{2\sigma_x^2}\right] \tag{5.3}$$

where σ_x denotes the standard deviation of the offset and x denotes the value of the offset. Using Equation 5.3, we can plot the graph of probability versus offset as shown in Figure 5.5, Using Figure 5.4 and Figure 5.5 a plot of probability versus efficiency

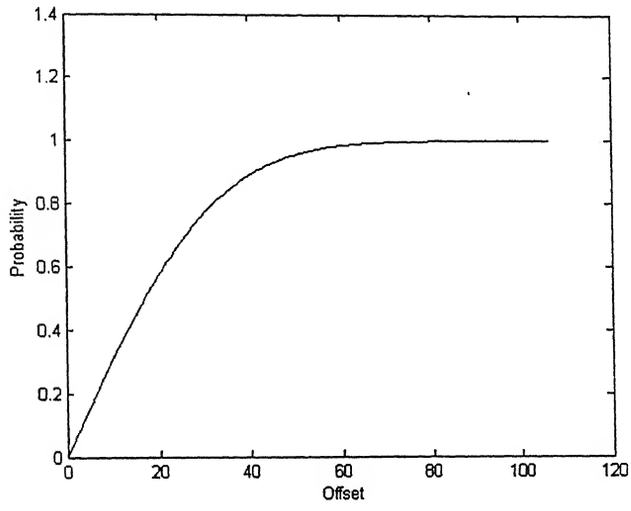

Figure 5.5: Probability versus offset (μm) for all the BOIs'

can be obtained as shown in Figure 5.6. The area under this curve gives the value of alignability.

5.2 Alignability of BOI-2

Referring to Figure 5.2, the emitter plane is first lens and the mirror is acting as the receiving plane. The total power in the beam transmitted from the first lens is equal the power coupled to the first lens when there is no misalignment and is calculated in §4.1. The intensity distribution $U(x_3, y_3)$ has been given by Equation 4.8 and shown

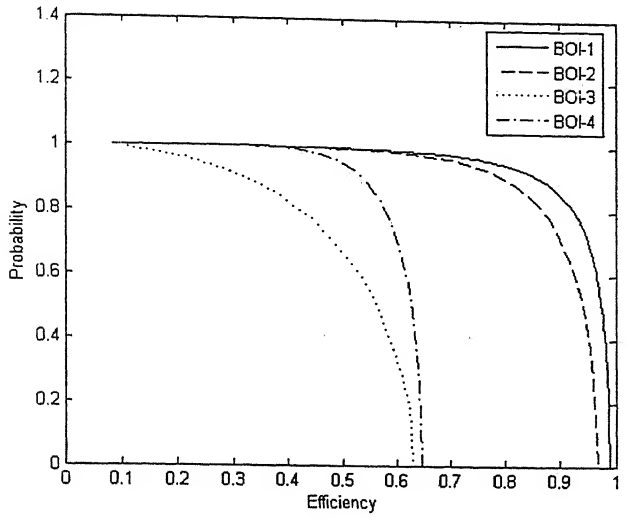

Figure 5.6: Probability versus Efficiency for all the BOIs'

in Figure 5.7. where I_m is intensity distribution. Efficiency of BOI-2 is given by Equation 5.4,

$$\eta_{BOI-1} = \frac{Power\ coupled\ to\ the\ mirror}{Total\ power\ in\ the\ beam\ transmitted\ through\ first\ lens} \tag{5.4}$$

It has been assumed that only transverse offset occurs in the mirror. Figure 5.4 and Figure 5.5 shows a plot of efficiency versus offset and probability versus offset obtained using the same procedure as for BOI-1. The variation of probability versus efficiency can now be drawn as shown in Figure 5.6. The area under this curve gives the value of alignability.

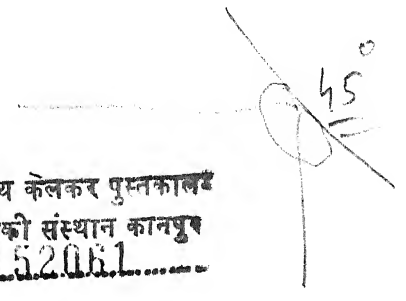

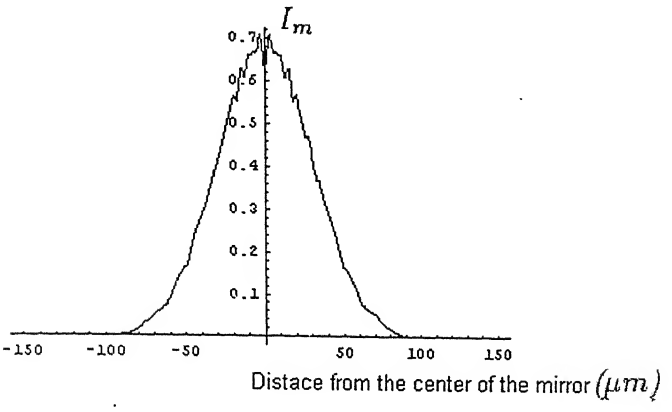

Figure 5.7: Intensity distribution on mirror

5.3 Alignability of BOI-3

For BOI-3, the emitter plane is the finite aperture of mirror and the receiving plane is second lens. We have assumed only a angular offset in the mirror because of which the efficiency of BOI-3 wll decrease. The efficiency of BOI-3 is defined as,

$$\eta_{BOI-1} = \frac{Power\ coupled\ to\ the\ second\ lens}{Total\ power\ in\ the\ beam\ reflected\ from\ the\ mirror} \tag{5.5}$$

Because the mirror is misaligned them beam shape changes its distribution and looses its circular symmetry, but because the misalignment is very small so for the convenience of calculation we assumed that even after reflection from the mirror the intensity distribution of the beam is circularly symmetric. The effect of misalignment is only the change in the direction of propagation of beam and can be understood by a simple example. Assume that we have a source of light emits gaussian beam with a mirror at 45 degree inclination. After reflection from mirror the beam fall on the detector. The

gaussian beam from the source is given by the expression,

$$U(x_1, y_1, z_1) = A\left\{\frac{w_0}{w(z)} exp\left[-\frac{r^2}{w_z^2}\right]\right\} \times exp\left\{-j\left[kz - \arctan\frac{z}{z_0}\right]\right\} \times exp\left[-j\frac{kr^2}{2R(z)}\right] \quad (5.6)$$

The dependence of the efficiency on angular misalignment can be calculated by performing a co-ordinate transformation on the gaussian optical beam described above. We suppose that the angle of the micromirror is misaligned by $\theta/2$,resulting in an angular misalignment of θ of the optical beam, as shown in Figure 5.8. Furthermore

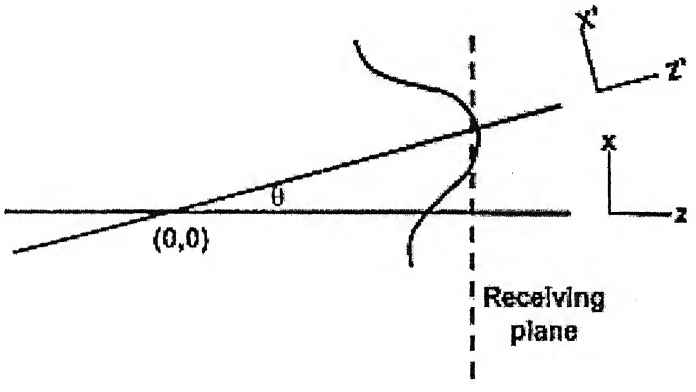

Figure 5.8: Drawing depicting angular misalignment of the optical beam with respect to receiving optics

if the distance from mirror to source plane and the transmitter plane is *d1* and *d2* respectively,the wave function of the optical beam after the micromirro now becomes

$$U(x_1, y_1, z_1) = A\left\{\frac{w_0}{w(d_1+z')} exp\left[-\frac{x'^2+y^2}{w^2_{d_1+z'}}\right]\right\}$$
$$\times exp\left\{-j\left[k(d_1+z) - \arctan\frac{d_1+z'}{z_0}\right]\right\}$$
$$\times exp\left[-j\frac{x'^2+y^2}{2R(d_1+z')}\right] \tag{5.7}$$

The coordinate (x',z') is related to original (x,z) coordinates by

$$x' = x\cos(\theta) - z\sin(\theta)$$
$$z' = x\sin(\theta) + z\cos(\theta) \tag{5.8}$$

Using the same method we can calculate the effect of angular misalignment in the mirror on the efficiency of the BOI-3. In BOI-3, the beam profile reflected from mirror is not gaussian in nature but is given by $U'(x_4, y_4)$ given by Equation 5.9,

$$U'(x_4, y_4) = U(x_3, y_3)P_m \tag{5.9}$$

where P_m is the pupil function of mirror as defined in §4.3 and $U(x_3, y_3)$ is given by Equation4.8. When there is no misalignment the intensity distribution on the second lens is shown in Figure 5.9. For different angle of misalignment, we can find the amount of power coupled on the second lens and hens the efficiency. A plot efficiency versus angular offset in the mirror is shown in Figure 5.10 A plot of probability versus angular offset can be drawn and hence the plot of probability versus efficiency plot as shown in Figure 5.6.The area under this curve gives the value of alignability.

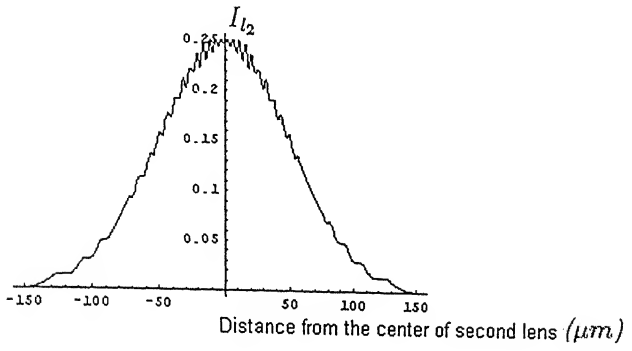

Figure 5.9: Intensity on second lens

5.4 Alignability of BOI-4

BOI-4 consists of second lens as source plane and detector as the receiver plane as depicted in Figure5.2. The total power transmitted through second lens is equal the power coupled to the second lens when there is no misalignment and is calculated in §4.4. The intensity distribution on the detector $U(x_5, y_5)$ has been given by Equation 4.12 and shown in Figure 5.11. where I_d is intensity distribution. Efficiency of BOI-4 is given by Equation 5.10,

$$\eta_{BOI-4} = \frac{Power\ coupled\ to\ the\ detector}{Total\ powerin\ the\ beam\ transmitted\ through\ second\ lens} \tag{5.10}$$

It has been assumed that only transverse offset occurs in the mirror. Figure 5.4 and Figure 5.5 shows a plot of efficiency versus offset and probability versus offset obtained using the same procedure as for BOI-1. The variation of probability versus efficiency can now be drawn as shown in Figure 5.6. The area under this curve gives the value of alignability.

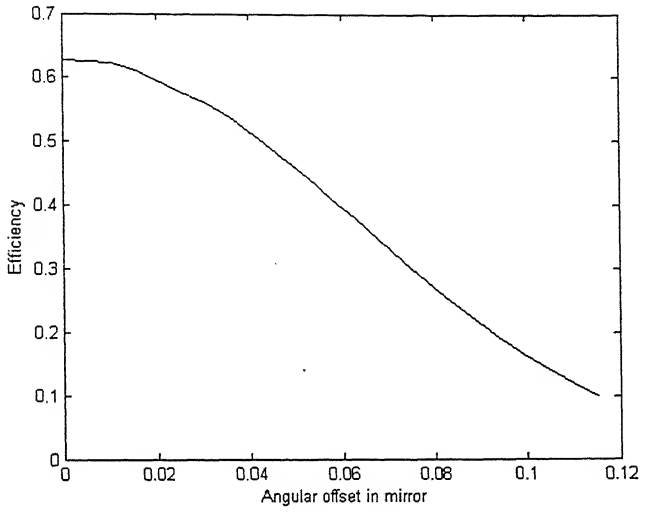

Figure 5.10: Efficiency versus angular offset in mirror ($\mu degree$)

5.5 Analysis of results

The simulation results can be broadly classified into two parts,

In the first part we have calculated the alignability of a practical optical interconnect. Solving for the amplitude distribution of laser beam at different positions of the optical interconnect accurately is a tedious process, with the assumption that there exists a near field diffraction and also that the effect of truncation due to small aperture of optical component is noticeable. Furthermore, calculating the power coupled with the different optical components is a time consuming process. With all these complication, computing the alignability values is not a trivial problem.

We have plotted the curves between Probabilities versus Efficiency for all the BOIs of the practical optical interconnect with following specifications.

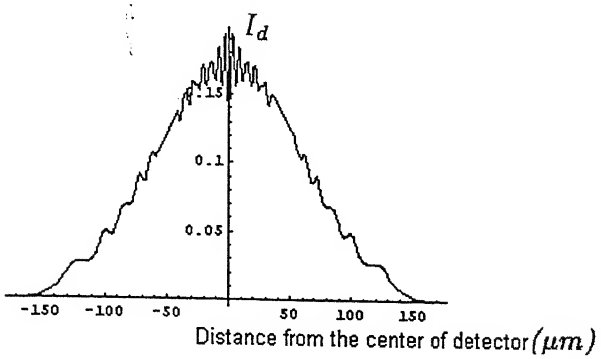

Figure 5.11: Intensity distribution on detector

Wave Length (λ) = $0.67\mu m$,

Beam Radius (w_0) = $50\mu m$,

Distance of first lens from Source (z_{fl}) = $550\mu m$,

Distance of mirror from first lens (z_m) = $550\mu m$,

Distance of second lens from mirror (z_{sl}) = $550\mu m$,

Distance of detector from second lens (z_d) = $550\mu m$,

Focal length of first lens (f_{one}) = $250\mu m$,

Focal length of second lens (f_{two})= $250\mu m$,

Aperture radius of first lens (r_{fl})= $75\mu m$,

Aperture radius of mirror (r_m) = $75\mu m$,

Aperture radius of second lens (r_{sl}) = $75\mu m$,

Aperture radius of detector (r_d) = $60\mu m$,

Standard deviation of transversa offset (σ_t)=$25\mu m$.

Standard deviation of angular offset (σ_a)=5_{ℓ} *degree*.

Area in plot between probabilities versus efficiency gives the value of alignability of the respective BOI. The value of alignability is given by,

Alignability of BOI-1 is = 0.84630

Alignability of BOI-2 is = 0.8236

Alignability of BOI-3 is = 0.4155

Alignability of BOI-4 is = 0.5104

The overall alignability of the optical interconnect is the multiplication of the individual alignabilities and is equal to 0.1478.

We now change the different parameters of optical interconnect like distance between different optical components, focal length of the lens, radius of the aperture of optical component *etc* and calculate the value of alignability for different setups. Comparing the value of alignability of the different setups, we can get an idea as to which setup is easy to align. A higher value of alignability indicates an easy with which an optical interconnect can be aligned.

In the second part, we have calculated the percent change of alignability by changing the values of the parameters by $\pm 10\%$ from its initial values. A change in the value of a parameter is attempted, keeping other parameter constant. The results in percent change in the alignability are as follows,

Parameters of interconnect	%Change in alignability (-10% change in parameter)	%Change in Alignability (10% change in parameter)
w_0	- 24.74	13.62
z_{fl}	- 0.87e-1	$0.93e^{-1}$
z_m	- 11.163	4.38
z_{sl}	- 5.58	$- 0.85e^{-1}$
z_d	-29.78	20.11
r_{fl}	0.26	- 2.34
r_m	0.21	- 7.21
r_{sl}	-1.02	- 6.22
f_{one}	12.88	- 18.81
f_{two}	15.67	- 15.52

We can see that the alignability is not equally sensitive to all the parameters. There are only few a parameter which change the value of alignability significantly. In our setup those parameters are,

1. Beam width of the source.
2. Focal length of first lens.
3. Focal length of second lens.
4. Distance between second lens and detector.

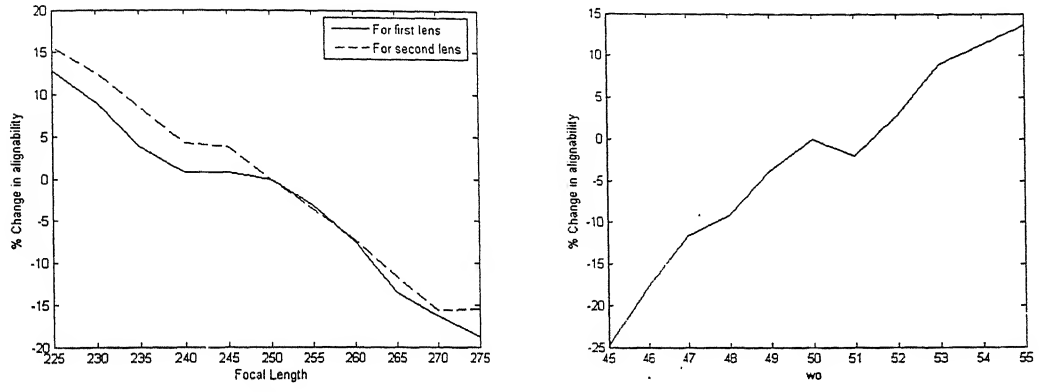

Figure 5.12: % change in alignability from its inetial value with changing values of focal length(μm) and beam width(μm)

For a optical interconnect, if we want to alter the parameters is such a way that its alignability can be maximize, we need not to alter all the parameters but only those parameters on which alignability depends the most can be manipulated for achieving higher alignability. The plot of percent change in alignability from its initial value with respect to change in different parameter is shown in Figure 5.12, the alinability value changes gradually with the change in focal length and beam width.

5.6 Conclusion

This thesis extends the alignability definition of a practical optical interconnect, using the alignability value we can compare different setups of optical interconnect and can choose the best out of them. Also the sensitivity of alignability with respect to the different parameters can be used to optimize the design of an optical interconnect more

effectively.

5.7 Recommendation for future work

Optical interconnect proves to be a promising technology that could emerge as a new architecture for the next generation of information processing systems. Much work still has to be done to make this a suitable technology.

Although in this thesis, only the alignability of a single optical interconnect was analyzed, the alignability discussed here could be extended for a array of optical interconnects in fact any optical or optoelectronics system consists of interconnects so the alignment issue is of prime importance for any kind of optical system. With slight alteration we can extend alignability definition for any optical setup in order to realize a reliable and low loss system.

Appendix A

Accuracy of numerical integration

We can not get the closed form solution of the integrations used for calculating the power coupled with optical component of the interconnect. For solving these integrations use the Simpsons method of numerical integration. For applying Simpsons method we have used Mathematica as a tool.

For checking the accuracy of the program written in mathematica, we have compared a few known results for a integral with the results we get from our program for the same integral.

Consider a Gaussian beam passing through a collimating lens and focused at a point, as illustrated in Figure A.1.

In the first case, we are assuming that the lens is an ideal lens, *i.e.* is all the power contained in the incident beam is transmitted through the lens without any loss. If W_{in} is the beam width of Gaussian beam before focused by a lens, after focusing from

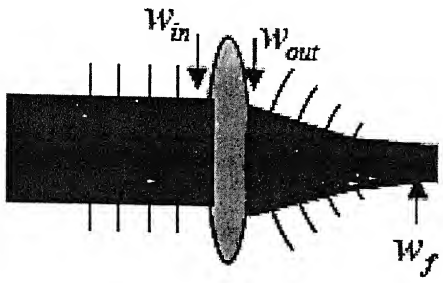

Figure A.1: Gaussian beam passing through a lens

the lens the beam width at the focus of the lens is given by Equation A.1.

$$W_f \approx \frac{f\lambda}{\pi W_{in}} \tag{A.1}$$

Before and after transmission through lens, nature of intensity profile of the beam remain gaussian.We can calculate the maximum intensity value of focused beam at its center by using Equation A.2.

$$I_{f_{max}} = I_{in_{max}} \left(\frac{W_{in}}{W_f}\right)^2 \tag{A.2}$$

Assuming $I_{in_{max}}$ is equal to 1, value of W_{in} is $85\mu m$, value of focal length(f) of the lens is $425\mu m$ and wave length(λ) of the gaussian beam is $.67\mu m$, then the value of $I_{f_{max}}$ will be equal to $6347.4\mu m$.

In the second case, We know the amplitude distribution of the gaussian beam just behind the mirror is given by Equation 4.1 and using transformer formula as given by Equation 3.2 we can find the amplitude distribution just after lens. Applying the near field diffraction formula and using our numerical integration technique we can find the amplitude distribution and hence the value of maximum intensity at the focus of the

lens. If the aperture of the lens is small in compare to the beam width of gaussian beam, maximum intensity value at focus of lens will differs from the value of intensity as find in previous case when it has been assumed that the aperture of lens is infinite. If we increase the the value of the radius of aperture of lens, the truncation of beam due to short aperture will decrease and the maximum intensity value in both the cases should become equal.

We have check the intensity value for both the cases ,the results are given by the given table.

As we can see as the size of lens aperture is increased the difference of intensity by two method is decreased and finally the error come down to 0.08%. We can claim that the error in Simpson numerical integration technique is near to 0.08%

Radius Of lens	Max.intensity for main lobe (for ideal lens)	Max. intensity for main lobe (using Simpson)	% Error in intensities by two methods
100	6347.5	3567.96	43.78
120	6347.5	4739.28	25.34
140	6347.5	5537.89	12.75
160	6347.5	5990.93	5.61
180	6347.5	6210.52	2.15
200	6347.5	6303.09	0.69
220	6347.5	6337.39	0.16
240	6347.5	6348.64	0.01
260	6347.5	6351.92	0.07
280	6347.5	6352.77	0.08
300	6347.5	6352.96	0.08
320	6347.5	6353.00	0.08
1000	6347.5	6353.01	0.08

(All the units are in μm)

Appendix B

Validation of using Fresnel near field approximation

In this thesis for seeing the diffraction pattern at different positions of optical interconnect we have used the Fresnel-Kichhoff diffraction formula with near field approximation. For our setup of optical interconnect, we have estimated that for taking fresnel near field approximation the minimum distance between the component should be grater than $700\mu m$ but the value of distance we have taken originally is $550\mu m$. The difference between two distances is very less so it seems that the near field approximation will be applicable for our setup.

To show the accuracy of near field approximation for our setup, we have plotted the intensity pattern on the microlens of our optical interconnect(Figure 1.2)using the Fresnel-Kirchhoff formula, with and without near field field approximation as illustrated in Figure B.1 and Figure B.2 respectively.

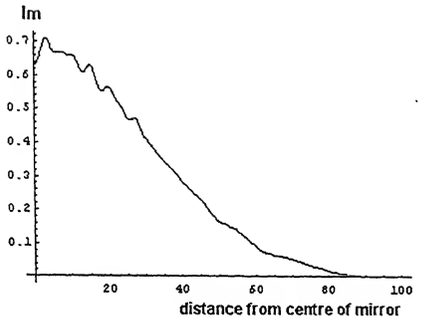

Figure B.1: Intensity distribution on the mirror using Fresnel-Kirchhoff formula

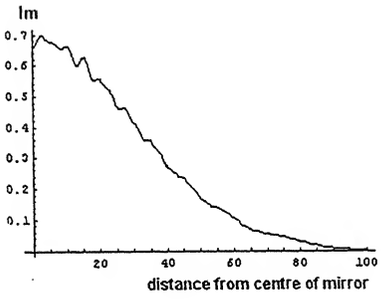

Figure B.2: Intensity distribution on the mirror using Fresnel-Kirchhoff formula with near field approximation

Where I_m is value of intensity. Seeing the resemblance of intensity distribution of these two plots it can be claim that diffraction pattern get by applying directly Fresnel-Kirchhoff formula and with near field approximation is same in nature.

References

[1] Anjan K. Ghosh, "Alignment Consideration in the Package Design of Optical Interconnect System," *IETE:Technical Review* , vol. 13,No. 3, pp. 163–177, May-June 1996.

[2] Keigo Iizuka, *Element of Photonics* , vol. 1. New York: John and Wiley & Sons, 2002.

[3] Joseph E. Goodman, *Introduction to Fourier Optics*: McGRAW - HILL BOOK COMPONY, 1973.

[4] Timothy P. Kurzwega, Steven P. Levitana, Jose A. Martineza, Philippe J. Marchandb, Donald M. Chiarullic, Diffractive Optical Propagation Techniques for Mixed-Signal CAD Tools.

[5] Y. S. Liu, B. Robertson, D.C. Plant, "Alignament Tolerecing analysis for on-axis non-telecentric free space optical interconnect" in *CLEO'96*.

[6] Suning Tang, Ray T. Chen, Lara Garrett, Dave Gerold, and Maggie M. Li, "Design Limitations of Highly Parallel Free-Space Optical Interconnects Based on Arrays of

Vertical Cavity Surface-Emitting Laser Diodes, Microlenses, and Photodetectors" *Journal Of Lightwave Technology*, Vol. 12, No. 11, November 1994.

[7] Samir Mezouari and Andy Robert Harvey, "Validity of Fresnel and Fraunhofer approximations in scalar diffraction" *Journal of Optics A: Pure and Applied Optics*, vol. 5, pp. 86–91, 2003.

[8] Andrew G. Kirk, Member, IEEE, David V. Plant, Member, IEEE, Michael H. Ayliffe, Marc Chteauneuf, and Frdric Lacroix, "Design Rules for Highly Parallel Free-Space Optical Interconnects," *IEEE journal of selected topics in Quantum Electronics*, , Vol. 9, No. 2, March/April 2003

[9] Bahaa E. A. Saleh, Malvin Carl Teich, *Fundamentals of Photonics*: John Wiley & Sons, Inc., 1991.

[10] Marc Finot, McDonald, William B. Chapman, poration Delin Li, Marc Epitaux, Zbinden, Jeff Bennett, J. Kozlovsky, Jean-Marc Verdiell, , "Automated Optical Packaging Technology for 10 Gb/s Transceivers and its Application to a Low-Cost Full C-Band Tunable Transmitter"*Intel Technology Journal*, vol 8, Issue 2. 2004.

[11] Mauro J. Kobrinsky, Bruce A. Block, Jun-Fei Zheng, Brandon C. Barnett, Edris Mohammed, Miriam Reshotko, Frank Robertson, Scott List, Ian Young, Kenneth Cadien, "On-Chip Optical Interconnects," *Intel Technology Journal*, vol. 08, issue 02, May 10, 2004.